Continual Evolution in Nonreciprocal Ecological Models

Aditya Mahadevan
Department of Physics, Stanford University, Stanford, CA 94305, USA

Daniel S. Fisher
Department of Applied Physics, Stanford University, Stanford, CA 94305, USA

(Dated: October 9, 2024)

Feedbacks between evolution and ecology are ubiquitous, with ecological interactions determining which mutants will be successful, and these mutants in turn modifying the community structure. We study the evolutionary dynamics of a number of ecological models with overlapping niche structure, including consumer resource and Lotka Volterra models. Evolution is slow, with ecological dynamics reaching a fixed point between successive introductions of invaders or mutants. When new strains are added to the community, either from an external pool or by large-effect mutations from parents within the community, the system converges, after an initial evolutionary transient, to a diverse eco-evolutionary steady state in which biodiversity continues to turn over at a constant average rate, without the invasion probability of new invaders getting any smaller. For resource-mediated interactions, this "Red Queen" phase of continual evolution obtains for any amount of asymmetry in the interactions between strains, while for generalized Lotka Volterra interactions, the evolutionary dynamics exhibit two eco-evolutionary phases as a function of interaction symmetry: for sufficiently asymmetric interactions the Lotka Volterra model displays a Red Queen phase, while above a critical amount of symmetry, an "oligarch" phase emerges in which the evolutionary dynamics continually slow down and a substantial fraction of the community's abundance condenses into a handful of slowly turning-over strains. The Red Queen phase across models is robust to general fitness effects that contribute intrinsic advantages to the growth rates of strains, provided the distribution of these selective differences is narrow enough. Via a dynamical mean field theory framework valid in the limit of high-dimensional phenotype space, we can analytically characterize the Red Queen eco-evolutionary steady state for a particular limit of model parameters—scaling arguments also allow an understanding of the nature of this phase and transients toward it across a broader range of parameter space. This work thus establishes a simple model of continual evolution in an ecological context *without* host-pathogen interactions, and points to the generality of such an eco-evolutionary phase.

CONTENTS

I. INTRODUCTION

Ecological and evolutionary processes are inextricably linked. In diverse microbial communities with large population sizes, there is constant interplay between ecological interactions and new mutations. Evolution continually creates new variants that interact with the community differently from their parent strains, and these eco-

logical interactions determine the fate of the new mutants and impact other species, thereby influencing future evolution. As the increasing body of data from natural microbial communities shows, microbes live in close proximity with one another, with multiple strains and substrains of the same species coexisting in many natural environments [1–3]. Understanding how ecological interaction webs influence evolution—and vice versa—is crucial to developing a richer picture of microbial evolution in both experimental and natural settings. A major puzzle is the ubiquity of closely related coexisting microbial strains, as evinced by the broad distribution of genomic divergences found within cells apparently occupying the same ecological niche [4, 5]. How does such diversity evolve and persist without clear ecological differences stabilizing the coexistence of strains? Theory is needed to develop scenarios for the evolution and maintenance of fine-scale biodiversity in large populations.

Even in controlled laboratory experiments with initially-clonal microbial populations, the development of ecology is inevitable. Although *apparent* selection pressures in the laboratory can be held constant, evolution in "simple" environments still results in the diversification and coexistence of different strains [6, 7]. Long after fitness—as measured by competition with the ancestor—has slowed in its increase and populations seem to be well adapted to laboratory conditions, evolution continues without a substantial decrease in the rate of beneficial mutations rising to a large fraction of the population [8]. Diversification and coexistence of lineages appears to be generic even in experiments *designed* to be simple enough to eliminate ecological effects, such Richard Lenski's long term evolution experiments in *E. coli* [8, 9]. Remarkably, even in laboratory experiments of bacterial populations without an external nutrient supply which might *a priori* be expected to exhibit severe resource limitation and diversity collapse, diversification and phenotypic turnover is found to continue over a timescale of years [10].

With interacting bacteria and phage populations, there is clear evidence—both experimental and observational—for the continual turnover and diversification of microbial lineages [11–13]. The "Red Queen hypothesis" [14] is often invoked to describe such arms-race evolutionary dynamics of hosts and pathogens. In this work we use the term more generally to describe the continual turnover of biodiversity in a community, without successful invasions of new mutants becoming rarer.

Inspired by such observations of microbial populations, we aim to understand what generic scenarios can emerge in the long term dynamics of evolution in ecological communities. We are particularly interested in robust behaviors which obtain across a range of parameters and models—such "phases" of eco-evolutionary dynamics present a set of qualitative possibilities that can be compared with experiment or observation. The phases that we study emerge in the limit of large biological complexity and therefore high-dimensional phenotype and interaction spaces upon which evolutionary and ecological processes play out. Looking for phases which are robust in the limit of high phenotypic dimensionality increases the likelihood that the conclusions that we draw might be somewhat universal and therefore relevant to natural systems, which are more complex—in multiple ways—than the simple models we study.

What long term behaviors emerge in high-dimensional eco-evolutionary models? In order to answer this question, it is useful to first think separately about the dynamics of evolution and ecology, initially in a well-mixed population with no spatial structure. A further simplification is natural for large microbial populations: that the dynamics is essentially deterministic, with demographic fluctuations negligible except in allowing for the possibility of extinctions.

In a static environment without ecology, gradual evolution of a large almost-clonal population can be caricatured as gradient ascent on a complex fitness landscape. The fitness landscape is a map from some high-dimensional organismal phenotype to a measure of reproductive success—the "fitness"—a misleading term as it is surely not a single quantity, except in the simplest non-ecological contexts. The emergence and fixation of beneficial mutations drives the population to high-fitness regions of phenotype space and evolution slows down as the population approaches one of many local maxima of the fitness landscape [15]. In high dimensions, the phenotype will generally spend a long time wondering around saddles before "committing" to a particular maximum, which is likely to be only marginally stable [16].

In large populations with an abundant supply of mutations the evolutionary dynamics of the population of genotypes is complex, with simultaneous exploration of multiple phenotypic directions, which has not been much explored theoretically. However if there is no ecology—except resource limitations capping the total population size—eventually the supply of beneficial mutations will become so limited that the population will again become almost clonal. By contrast, in an extrinsically changing environment, the fitness landscape depends on time, and is more accurately a "seascape." Not surprisingly, a continually changing environment can lead to evolutionary dynamics and sustained diversity which proceeds indefinitely without slowing down [17], however again this regime has not been much studied for large populations in high dimensions.

Just as evolutionary dynamics of large populations in high dimensions can display rich behavior even without ecology, ecological dynamics with no evolution can also exhibit various behaviors, with globally stable, multistable, and chaotic states all possible in simple models [18–20]. The most-studied contexts are ecological dynamics of *top-down assembled* communities, which consist of a large number of species brought together with their abundances obeying some fixed ecological dynamics. The simplest ecological phase that obtains at long times is a stable state in which species abundances reach a globally attracting stable fixed point with some number of species having nonzero abundance—a stable community—and the rest going extinct and being unable to re-invade even if reintroduced. As the diversity of the initial assembled community increases, this stable phase can yield to a more complicated behavior exhibiting multiple attractors and transient chaos, which remains only partially understood [18, 20, 21]. Chaotic fluctuations in this high-diversity unstable phase lead to many extinctions and the system settles down to one of many possible stable communities or limit cycles, but these states are

generically invadable by some of the extinct strains. A population of dormant spores that germinate and resuscitate extinct populations—or spatial heterogeneity which allows chaos to desynchronize across space—can sustain the chaos for times exponentially long in the lifetimes of the spores or the spatial extent of the system, respectively [22].

To bring evolution and ecology together, we focus here on the slowly evolving limit in which the ecological dynamics is much faster than the evolutionary dynamics and spatial mixing is fast enough to be ignored. This regime is the hardest in which to find sustained diversity and continual evolution because the short-term coexistence driven by continual invasions of new mutants, studied in refs. [23–25], will not occur. We study models in which the ecological dynamics is the simplest: convergence to a (usually) globally attracting fixed point some strains having gone permanently extinct. Under slow evolution, do the resulting eco-evolutionary dynamics remain diverse and continually turn over in a "Red Queen" steady state, or does evolution get progressively slower? Do generalist mutants take over and cause the diversity to crash? Are there multiple different phases of eco-evolutionary dynamics for different parameter choices?

It has been shown that Red Queen dynamics emerge generically in models of an almost-clonal population evolving in a high-dimensional fitness landscape with a small amount of environmental feedback [16]. Here the fitness landscape—now better caricatured as a "snowscape"—changes in response to the evolving population. For even a small amount of environmental feedback, the population wanders through phenotype space without settling down to a stable fixed point, due to selective forces that arise from the gradient of the fitness landscape as it is gradually modified by the feedback between the organisms and their environment. Universality emerges in these models in the limit of large phenotype dimension, with different microscopic models displaying similar phase diagrams [16].

In the eco-evolutionary models we study here, ecology acts—loosely—as a manifestation of feedback between organism and environment, with the "environment" of any particular strain set by its interactions with the rest of the community, and this environment subject to change every time a new beneficial mutant arises in the community. Do natural models of this process result in a Red Queen phase of evolution? If so, what sets the diversity of the community in this phase?

Some previous work has found that ecological communities, although capable of sustaining extensive diversity through standard mechanisms of resource competition [26] lose much of their diversity when they start to gradually evolve either by small mutations or by the introduction of independent species [27, 28]. These results were argued to deepen the puzzle of the extensive diversity observed in nature. However, the models in which such results have been reported are complicated enough that analytical understanding is difficult, and generality of the results is not clear.

The evolutionary process we study involves slowly adding strains one by one with extinctions permanent when they occur. The permanence of extinctions means that, once extinct, a strain will never have a chance to re-emerge, even if conditions become favorable for its growth. Therefore the order in which strains are introduced influences the fate of the community. However, the *statistical* properties of the community for large D depend only on the pool from which invaders are drawn, rather than the specific properties of the invaders.

Some recent work has incorporated evolution into ecological models without permanent extinctions [29]: here re-invasion of previously-extinct strains is possible if conditions later become favorable for them. This process eliminates the important difference between communities assembled all at once (top-down) and gradually (bottom-up), the latter of which is our focus.

A large amount of work by theoretical ecologists and statistical physicists has focused on ecological models that are sometimes tractable but nongeneric because they admit a Lyapunov function which is always increasing under the eco-evolutionary dynamics [30–32]. The existence of such a Lyapunov function depends on the symmetry of ecological interactions [33]—e.g. through perfect efficiency in the conversion of nutrients to biomass—which does not hold in biological systems. Therefore the robustness of conclusions drawn from such models is unclear. In the current work we focus on generic behavior, drawing conclusions away from the special region of parameter space with a Lyapunov function. Indeed we will show that, under evolution, the behavior of models with a Lyapunov function is qualitatively different from the general case.

Several other studies [34, 35] have noted the importance of *non-reciprocal* or *asymmetric* ecological interactions for reaching a state of continual evolution—we will provide further evidence for this conclusion in the high-diversity limit, which complements the more often-studied low-diversity case [34].

We are interested in dynamics of closely related strains, where differences between strain interactions with one another are the sum of many positive and negative effects. To caricature this biological complexity, we parameterize the strain-to-strain differences in phenotypic properties as random variables drawn from some distribution. This approximation of unknown complexity by randomness is a useful way to get a sense of general patterns of behavior that might apply across a range of ecological-evolutionary situations [36].

In the simplest models, strains interact with one another *directly*, with all pairwise interactions chosen from some specified ensemble. These models, which include generalized Lotka-Volterra interactions [18], suffer from a lack of strain phenotypes, which determine how each strain interacts with any other prospective strain. As a result, such Lotka-Volterra models do not admit a straightforward way of drawing random mutants that are correlated with a parent strain already in the community [37]. Nonetheless we can study the Lotka-Volterra dynamics in the case of independent invaders drawn from a fixed ensemble and added to the community, and we will show that this limit is useful for more generally understanding evolution driven by mutant strains that are correlated with their parents.

To explicitly study the effects of parent-mutant correlations, and to assess the generality of the qualitative phases of evolution that we find, we introduce structure into the

ecological interactions: specifically considering the case where they are mediated by a collection of chemicals (or resources) in the environment. Each strain has a phenotype which governs its interactions with the resources—both how they affect the strain and how the strain affects the resources—and therefore with all other strains. Small mutations then correspond to having highly correlated parent and mutant phenotypes, with the similarity between mutant-invader and parent in the community an important parameter.

The phenotype of each strain in such consumer resource models is given by its growth and consumption rates for each of the resources. The number of resources—or more generally, interaction-mediating chemicals—is a key quantity that we will call D. This number sets the *dimensionality* of the environment and of the interactions between consumers. It also sets a natural scale for the number of strains that can coexist: in the models we study here, this diversity is bounded above by D and "high-diversity" means that the number of coexisting strains is $\mathcal{O}(D)$. The limit of large D is therefore biologically relevant, and will allow us to analyze statistical—hopefully universal—properties of the resulting eco-evolutionary dynamics.

When mutational effects are sufficiently large, we find that key aspects of the evolutionary dynamics are captured by the dynamics of bottom-up assembly (with extinctions), wherein phenotypically *independent* invaders enter the community serially. We therefore study the independent invader limit for a large fraction of this work, due to its tractability and apparent genericity. The understanding from our analysis of simplified models gives us qualitative insight into differences between a top-down-assembled and an evolved community, along with a framework for understanding the Red Queen phase that occurs more generally.

In order for the Red Queen phase to be robust, it must be stable to the presence of "general fitness" mutations which increase the growth rate of a strain *regardless* of the composition of the community. These general fitnesses appear naturally in models of resource competition, where they correspond to the growth rates of strains in isolation. Metabolic tradeoffs, which constrain the width of the general fitness distribution, are sometimes invoked to sustain high levels of diversity in ecological settings. These tradeoffs can be strict [38, 39] or—more realistically—allow some variation in the total metabolic budget [32]. Without strict tradeoffs, can consumer resource models evolve towards a diverse state in which the distribution of extant general fitnesses is narrow? Or does evolution constantly push into the tail of the general fitness distribution and fail to reach a steady state? Do generalist species emerge and reduce diversity by outcompeting other strains?

Our main result is that there exists a robust high-diversity Red Queen phase of eco-evolutionary dynamics across a range of parameters and models, displaying continual evolution and turnover of biodiversity. This Red Queen phase obtains both for independent invaders and evolution by mutations with substantial phenotypic effects. The Red Queen phase persists in the presence of general fitnesses, as long as their distribution decays fast enough, with the shape of the general fitness distribution controlling the probability of successful invasion in the steady state, but not otherwise limiting the diversity or its turnover.

II. CONSUMER RESOURCE MODEL

A. Ecological dynamics and stable communities

We first study a standard model of resource competition with D externally-supplied resources (or more generally, interaction-mediating chemicals), and an assembled population of S different strains that consume these resources. The ecological dynamics of this consumer resource (CR) model are

$$\frac{dn_i}{dt} = n_i\left(\sum_{\beta=1}^{D}\mathcal{G}_{i\beta}\mathcal{R}_\beta - d\right) \tag{1a}$$

$$\frac{d\mathcal{R}_\alpha}{dt} = K_\alpha - \mathcal{R}_\alpha\sum_{j=1}^{S}\mathcal{F}_{j\alpha}n_j - \omega\mathcal{R}_\alpha, \tag{1b}$$

where the $\{n_i\}$ are the populations of strains, labeled by Roman indices $i \in \{1, 2, \dots S\}$ and the $\{\mathcal{R}_\alpha\}$ are resource abundances labeled by Greek indices $\alpha \in \{1, 2, \dots D\}$. The resource supply vector $\mathbf{K}$ has components K_α, and d and ω are respectively the death rate of the consumers and the decay (or dilution) rate of the resources. Without loss of generality for our current purposes, we take all the K_α to be equal and given by a constant K, and we set $\omega = 0$ to reduce the number of parameters without changing the qualitative behavior. The $S \times D$ matrices $\mathcal{G}$ and $\mathcal{F}$ respectively parameterize the *growth* and *feeding* rates of each consumer on each resource: the phenotype of strain i is the corresponding row of $\mathcal{G}$ and $\mathcal{F}$ taken together, so that the dimensionality of phenotype space is $2D$. The elements of $\mathcal{G}$ and $\mathcal{F}$ consist of some positive mean—an average growth or feeding rate—in addition to a heterogeneous part that varies between strains and resources. Ref. [32] studied the ecological dynamics of a *symmetric* version of this model with $\mathcal{F} = \mathcal{G}$. Although we expect $\mathcal{G}$ and $\mathcal{F}$ to be positively correlated, some amount of asymmetry is generic, and we will show that this asymmetry is important for the dynamics we study.

For closely related strains, the differences between interactions will be sums of positive and negative effects—thus we treat $\mathcal{G}_{j\alpha}$ and $\mathcal{F}_{j\alpha}$ as random variables drawn from some distribution. With the interpretation of consumption and growth, one expects all elements to be positive, though a small fraction being negative (corresponding loosely to crossfeeding and/or inhibitory effects) does not change the behavior. For simplicity we draw the elements from gaussian distributions with means μ_g, μ_f and variances σ_g^2, σ_f^2 respectively. (The choice of a gaussian distribution is convenient as we will later take advantage of this structure to evolve strains by drawing from the ensemble of interactions conditional on inequality constraints.) We parameterize elementwise correlations between $\mathcal{G}$ and $\mathcal{F}$ by $\mathrm{Corr}[\mathcal{G}_{j\beta}, \mathcal{F}_{j\alpha}] = \kappa\delta_{jk}\delta_{\alpha\beta}$, where $\mathrm{Corr}[A, B]$ is the Pearson correlation coefficient, and the *symmetry parameter* $\kappa \in [0, 1]$ determines the similarity between growth and consumption rates. The ratios σ_g/μ_g and σ_f/μ_f determine what fraction of the entries of $\mathcal{G}$ and $\mathcal{F}$ are positive; it is

only these ratios that matter and we consider $\sigma_f \lesssim \mu_f$ and $\sigma_g \lesssim \mu_g$ so that most entries are positive. With the choice of $\omega = 0$ there are only three relevant parameters other than S and D: κ, σ_g/μ_g and σ_f/μ_f, with K setting a scale for the consumer abundances (Appendix A). Without loss of generality we set $\mu_f = \mu_g = 1$, $d = 1$ and $K = 1$.

The degree of correlation, κ, between the feeding and growth rates plays an important role. $\kappa = 1$ presumes identical efficiencies between strains of conversion between resources and biomass [32]. This symmetry guarantees the existence of a Lyapunov function (see Appendix A) that is always increasing along the ecological (and later evolutionary) dynamics of the CR model [33]. However for generic $\kappa < 1$ the dynamics do not have a Lyapunov function, and this distinction makes a big difference in the evolutionary dynamics, as we will see shortly.

We supplement the deterministic dynamics of Equation 1 with a small abundance threshold below which strains go *extinct*: their abundances are then set to zero and *cannot recover*. We exclude demographic fluctuations as we are interested in large populations with the dynamics and extinctions driven deterministically by growth rate differences. Starting from positive initial conditions, the strain abundances reach a fixed point with some fraction of strains going extinct and others persisting at nonzero abundance. We denote the *community of strains* with positive fixed point abundances as $\mathcal{C}$. For small enough S—less than some multiple of D—the fixed point is stable and cannot be invaded by any of the extinct strains. For large D, in the parameter ranges of interest, the stable uninvadable community is highly likely to be unique [33]. The breakdown of this uniqueness above a critical value of S (discussed for a related model in ref. [20]), will, as we discuss, not play a role in the evolving communities of interest here.

At the ecological fixed point of the CR dynamics, the abundances $\{n_i^*\}$ of the extant strains and the concentrations $\{\mathcal{R}_\alpha^*\}$ are determined by

$$\mathcal{R}_\alpha^* = \frac{K_\alpha}{\sum_{j\in\mathcal{C}} \mathcal{F}_{j\alpha} n_j^*} \tag{2a}$$

$$0 = \sum_{\alpha=1}^{D} \mathcal{G}_{i\alpha}\mathcal{R}_\alpha^* - d \text{ for } i \in \mathcal{C} \tag{2b}$$

$$n_j^* = 0 \text{ for } j \notin \mathcal{C} \tag{2c}$$

with the strains $j \notin \mathcal{C}$ extinct. The total population size, $N = \sum_i n_i^*$, is of order $\mu_g \sum_\alpha K_\alpha/\mu_f$, which is roughly D for our choice of parameters. (We have kept the dependence on $\mathbf{K}$ explicit because it carries a physical meaning and characterizes the environment. In our simulations all of its components are 1: the effects of changing $\mathbf{K}$ are discussed briefly in Section V.)

We define $L = |\mathcal{C}|$ as the number of extant strains *left* in the community at the ecologically stable fixed point. In accordance with the competitive exclusion principle [26], the maximum L that can stably coexist at a fixed point is D, as seen from the insufficiency of the fixed point conditions otherwise. For natural choices—including ours—of the ensemble of interactions, the typical number of strains that can stably coexist at a fixed point is less than D, but scales linearly with D. This linear relationship between the diversity of the community and the number of resource-mediating chemicals is expected to be generic across a range of consumer resource models with heterogeneous interactions, with the statistics of the interactions affecting the prefactor in the scaling [32]. In ecological language, the number of *potential niches* is D but not all of these can be filled.

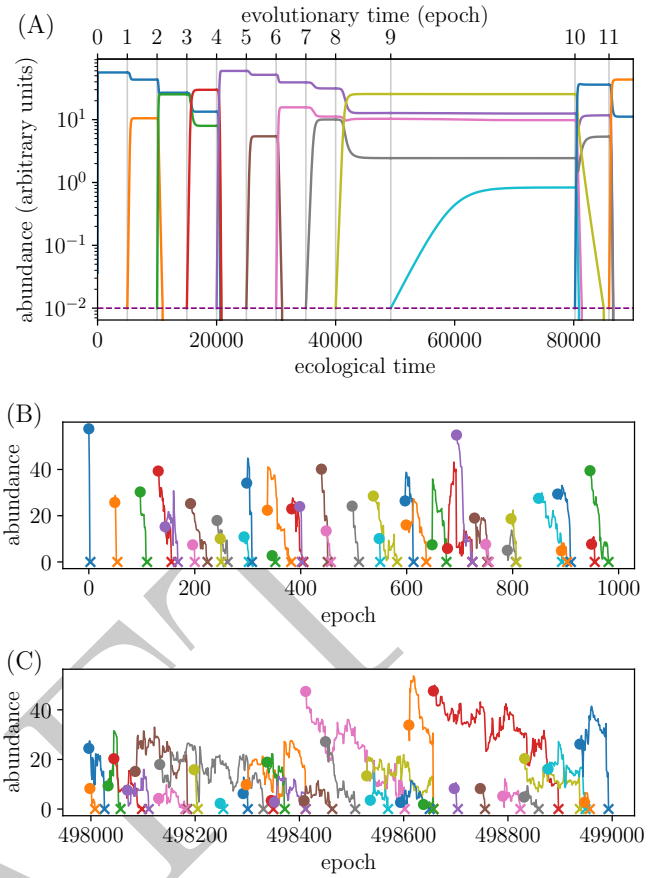

Figure 1. Strain abundances in the consumer resource (CR) model on ecological and evolutionary timescales. (A) Starting with a single strain, ecological dynamics reach a fixed point between each new strain invasion, which starts a new epoch. Ecological time, on lower axis; evolutionary time, in epochs, on upper axis. (B) Selected strain abundance trajectories evolutionary timescale, for first 1000 epochs. (C) Selected strain abundance trajectories after a long period of evolution. Turnover of diversity is slower than during initial stages of evolution, but converged to a steady average rate. Parameters are $\kappa = 0.4$, $D = 50$, $\mu_f = \mu_g = 1$, $\sigma_f = \sigma_g = 1/4$, $d = 1$, $\omega = 0$, $K_\alpha = 1$.

Given an ecological fixed point, whether a given strain added to the community can invade from low abundance is determined by the sign of its *invasion fitness*

$$\xi_i = \sum_{\alpha=1}^{D} \mathcal{G}_{i\alpha}\mathcal{R}_\alpha^* - d. \tag{3}$$

If ξ_i is positive, strain i can invade.

B. Evolution

Evolution by independent invaders: We now consider

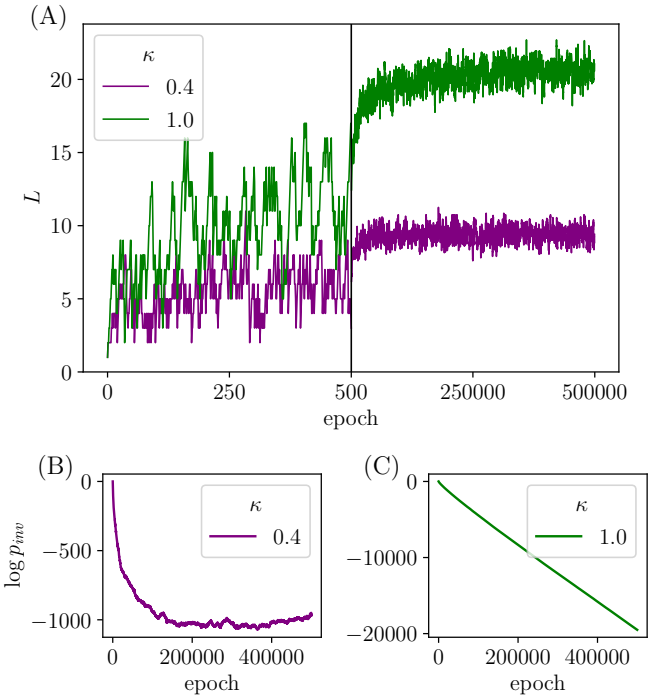

Figure 2. The CR model reaches a steady state for symmetry parameter $\kappa = 0.4$, but not for perfect symmetry, $\kappa = 1$. (A) Community diversity L as function of evolutionary time, starting from a single strain. The first 500 epochs shown on stretched scale; thereafter as a moving average over windows of 1000 epochs. L increases, then fluctuates around steady state for $\kappa = 0.4$, but creeps up for $\kappa = 1$. (B)–(C) The invasion probability decreases initially, then reaches steady state for $\kappa = 0.4$, but continues to decrease for $\kappa = 1$. The absurdly small p_{inv} is artifact of particular distributions of parameters. Parameters same as Figure 1 with $D = 50$.

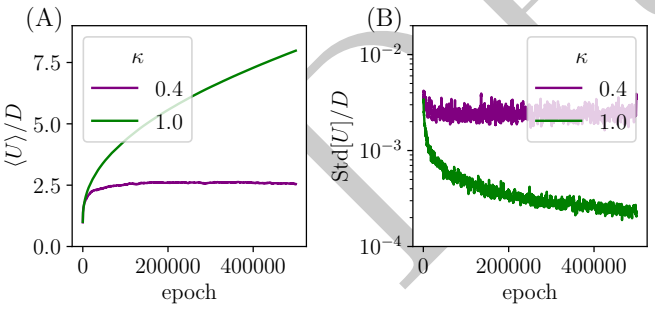

Figure 3. (A)–(B) The mean and standard deviation of the extant distribution of generalized fitness, U_i, over evolutionary time for $\kappa = 0.4$ and 1. Distribution stabilizes for $\kappa = 0.4$. For $\kappa = 1$, mean continues increasing with width decreasing. Parameters same as Figure 1

slow evolution of stable communities in the CR model where there is a clean separation of timescales between evolution and ecology: the ecological dynamics run until a fixed point is reached, and then a single new strain is introduced. The ecological dynamics again run until a fixed point is reached. We first study the simplest case of *independent invaders* into the community. Although this process could justifiably be called "bottom-up assembly," it will give us insight into evolutionary dynamics with large-effect mutations. We start with a single strain of consumer and a collection of D resources, and repeatedly add an unrelated consumer strain drawn from the gaussian ensemble of its phenotypic properties. We define an *epoch* as the unit of time corresponding to a *successful invasion* followed by a relaxation of the ecological dynamics to a fixed point. Although the length of an epoch in ecological time varies between epochs, if evolution is slow enough (as we assume here) the ecological timescale is not important for the evolution.

With each new strain added to the ecosystem, we find a stable ecological fixed point of the community either by integrating the dynamical equations with a small extinction threshold, or by the more efficient iterative algorithm described in Appendix D. Once L is sufficiently large, we expect that this fixed point is globally attracting from positive initial conditions with high probability, since it starts out this way, and the community changes by a small amount with each invasion. In particular, strains that have gone extinct during a given epoch will generally not be able to reinvade even if reintroduced.

In order for a new strain, labelled a, to be able to invade, it must have positive invasion fitness ξ_a. Furthermore, if it successfully invades, the fixed point abundance n_a^* will be proportional to ξ_a, with the constant of proportionality determined by the properties of the community into which a invades (as can be seen by a perturbative analysis for large L). The dot product between the growth vector $\mathcal{G}_a$ (the ath row of $\mathcal{G}$) and the resource vector $\mathcal{R}^*$ of the current community determines the invasion fitness of strain a. Therefore when we draw the phenotype of a—consisting of D-dimensional vectors $\mathcal{G}_a$ and $\mathcal{F}_a$—from their gaussian ensemble, we condition on $\xi_a > 0$, which allows us to drastically speed up numerics when the evolution pushes the extant distribution of interactions to have large mean, which makes the probability of drawing an invader with $\xi_a > 0$ very small [40].

The resource availability vector $\mathcal{R}^*$ can be thought of as a modified version of the supply vector $\mathbf{K}$, where the availability of resource α is reduced from K_α by a factor of $\sum_j \mathcal{F}_{j\alpha} n_j^*$. Therefore alignment between $\mathcal{G}_a$ and $\mathbf{K}$ results in a contribution to the invasion fitness of strain a that is independent of the other strains in the community—this contribution to the invasion fitness is a form of *general fitness* characterized by $U_i \equiv \sum_\alpha \mathcal{G}_{i\alpha} K_\alpha$, which captures the average performance of strain i against all of the D resources. The invasion fitness of strain i in the *absence* of all other strains is then $U_i - d$. Therefore ξ_a for an invader has a community-independent contribution from general fitness U_a as well as a community-dependent contribution from the ecological interactions of the particular extant community. We refer to the community-dependent part of the invasion fitness as the *drive*. It is useful for analysis to extend these definitions to strains in the community: for $i \in \mathcal{C}$ we define ξ_i as the growth rate strain i would have if it were removed from the community and then reintroduced at low abundance. This quantity arises naturally in the mean field description of ecological models (Appendix G and Section IV) and we will sometimes refer to it as the *bias*, consistent with previous work [22]. The bias can be roughly thought of as

an invasion fitness defined for strains already in the community, and differences between biases of different strains come from two pieces: the general fitnesses and the drives. Such differences are responsible for the differential growth and extinction of strains.

As we show in Appendix C, in a randomly assembled community the *selective differences*—differences between general fitness terms U_i—comprise the dominant contribution to the width of the bias distribution, larger by a factor of $\sqrt{D}$ than the contribution from the drives. For large D the selective differences between strains determine both the ecological and early-stage evolutionary dynamics. This is because the selective differences between strains are *first order* in the phenotypic differences, proportional to $\mathcal{G}_{i\alpha} - \langle \mathcal{G} \rangle$, with angular brackets denoting *community averages*, while the variations in the drives are second order, proportional to both $\mathcal{G}_{i\alpha} - \langle \mathcal{G} \rangle$ and $\mathcal{F}_{i\alpha} - \langle \mathcal{F} \rangle$. Previous work [32] has forced the contributions to be comparable by scaling the mean and variance of $\mathcal{G}$ and $\mathcal{F}$ as $1/D$, while in fact it is their mean and *standard deviation* that should be the same order in a biologically-motivated model. We will later show that in a long-evolved community, the variations in the general fitnesses become much smaller, indeed comparable to the variations in the drives, but this must be shown rather than assumed.

Figure 1A shows the ecological dynamics of the consumers from Equation 1, punctuated by well-spaced evolutionary events when each new invader comes in. The resource dynamics are taken to be fast enough that the resources are always instantaneously at their steady state: this does not affect the fixed point but makes visualization simpler. We start with a single strain ($S = 1$), and when the system is at a fixed point, we introduce a new strain, drawn randomly from ensemble with $\kappa = 0.4$ and $D = 50$ conditional upon its having positive invasion fitness. When the new strain joins the community, it perturbs the abundances of the other strains in the community, sometimes causing extinctions. (We have chosen $\kappa = 0.4$ for these simulations which is well away from $\kappa = 1$ for which there is a Lyapunov function: we investigate that special case further below.)

The changes caused by invading strains can be visualized over longer times by coarse-graining the time resolution from ecological to evolutionary times, as done in Figure 1B. Here we track the fixed point abundances of strains in the community for a much longer simulation that uses the algorithm in Appendix D. We show only a few of the strain abundance trajectories for ease of visualization. It is apparent that when strains come in, their abundances can fluctuate with further evolution but tend to decrease and do not last very long, rapidly driven extinct by subsequent invaders which are better adapted to the community-modified environment than they are. However, as shown in Figure 1C, the dynamics look substantially different after a long period of evolution (5×10^5 epochs). Late in the evolution, each introduced strain stays in the community for a larger average number of epochs, and the new invaders have a smaller general fitness advantage over the community mean, with an overall larger number of strains extant at any given time. As a result, the diversity turns over more slowly; the typical lifetime of a strain scales with the community size L.

A primary quantity of interest during the process of repeated invasion is the diversity of the community. In the case of independent invaders, the number of extant strains, L, is the most natural measure of the diversity of the community. At long times, L is roughly constant with $\mathcal{O}(\sqrt{L})$ fluctuations on evolutionary timescales (Figure 17), resulting from rough independence of strains along with robustness of the community to perturbations (Section IV B). In Figure 2A, we plot L as a function of evolutionary time for communities starting from a single strain with $\kappa = 0.4$. L initially grows fast and then slows down, appearing to saturate with ~ 10, strains coexisting at any given time, in—as we shall see—a Red Queen steady state.

For the special case $\kappa = 1$, also shown in Figure 2A, the diversity displays a longer transient and continues gradually increasing: it is therefore difficult, based only on the dynamics of L, to know whether a steady state obtains by the end of the simulation. However the presence of a Lyapunov function makes the behavior *qualitatively different* from that of $\kappa < 1$. When $\kappa = 1$, invading strains must increase the Lyapunov function Λ. Therefore even if L saturates, there cannot be a steady state. There is no absolute upper bound of Λ in the ensemble of all possible invaders, but the larger Λ gets, the more unlikely it gets to sample strains that can increase it further—thus the probability of invasion must steadily decrease. It is interesting to note that, in spite of this gradual increase of Λ, L stays far away from its upper bound of $D = 50$. Indeed, L stays below its maximum value of $D/2$ for a randomly *assembled* community with $\kappa = 1$ [32]—however it is not clear whether eventually L might exceed this bound.

Figures 2B and 2C provide evidence for the Red Queen steady state when $\kappa = 0.4$, and lack of steady state when $\kappa = 1$. For $\kappa = 0.4$, the probability of a new strain having positive invasion fitness, which we denote by p_{inv}, decreases at first and then reaches a steady state. Although the invasion probability for an invader is unrealistically small in the steady state ($p_{inv} \approx 10^{-400}$), a Red Queen state clearly obtains. In Section III A we introduce a family of models in which p_{inv} can be much larger for different parameter choices, and in Section IV E we discuss how the choice of the $\mathcal{G}$ and $\mathcal{F}$ ensembles affects the invasion probability at steady state: the tiny value here is an artifact of the gaussian ensemble.

By contrast, for $\kappa = 1$, the behavior of p_{inv} is clearly different, decreasing for the duration of the simulation and confirming the expectation that no Red Queen state exists.

We characterize the initial rapid adaptation and subsequent steady state (or lack thereof) in terms of the distributions of U_i in the community which play a particularly important role in the contrasting behavior for $\kappa = 0.4$ and $\kappa = 1$. Figures 3A and B show the mean and width of the extant U_i. For $\kappa = 0.4$, the mean of the U_i distribution, defined as $\langle U \rangle = \frac{1}{L} \sum_{i=1}^{L} U_i$, is initially increasing with the standard deviation of the U_i distribution decreasing, but after $\sim 2 \times 10^5$ epochs the distribution reaches a steady state. We shall show that the width of the distribution of extant general fitnesses is reduced by evolution until it is similar to the width of the distribution of drives—i.e. the community-dependent and community-independent parts of the bias

CR	consumer resource model (Equation 1)
LV	Lotka Volterra model (Equation 5)
ν_i	fractional abundance of strain i; $\sum_i \nu_i = 1$
S	number of strains in the initial community
L	number of extant strains in the community
D	number of resources mediating interactions
Q	niche parameter of LV model; $\mathrm{E}[V_{ii}] = -Q$
$\mathbf{K}$	vector of resource supply rates
$\mathcal{G}$	growth rate matrix
$\mathcal{F}$	feeding rate matrix
G	matrix of growth rate differences; mean 0
F	matrix of consumption rate differences; mean 0
V	pairwise strain interaction matrix
κ	$\mathrm{Corr}[G_{i\alpha}, F_{j\beta}] = \mathrm{Corr}[\mathcal{G}_{i\alpha}, \mathcal{F}_{j\beta}] = \kappa\delta_{ij}\delta_{\alpha\beta}$
γ	symmetry parameter for LV model; $\mathrm{Corr}[V_{ij}, V_{ji}] = \gamma$
U_i	$U_i = \sum_\alpha \mathcal{G}_{i\alpha} K_\alpha$
$\mathbf{R}$	linearized resource vector; $R_\alpha = -\sum_j F_{j\alpha}\nu_j$
p_{inv}	probability of an invader successfully invading
ξ_i	invasion fitness/bias
ζ_i	drive/community-dependent component of bias
Υ	community mean fitness; $\Upsilon = \sum_i \nu_i(s_i + \sum_j V_{ij}\nu_j)$
s_i	general fitness; intrinsic component of bias
Σ	scale of s distribution
$\Delta(\Upsilon)$	scale of s distribution for $s \approx \Upsilon$ (Equation 18)
ρ	correlation between parent and mutant

Table I. Definitions of commonly used variables and terms.

contribute similarly to bias differences. Once this occurs, the distribution of extant U_i stops pushing into the tail of its distribution and we reach a Red Queen evolutionary steady state with continual, roughly steady, turnover.

By contrast, for $\kappa = 1$, there is no steady state reached for the length of the simulation, and increase of Λ tracks the increase of $\langle U \rangle$ while the distribution of the U_i continues to narrow.

Evolution via mutations: So far we have considered independent invaders in the CR model. In Appendix B we also look at the evolutionary dynamics when invaders are correlated with a parent strain (chosen with probability proportional to its abundance) from the community. Indexing the parent by P and the mutant by M, we introduce a parameter $\rho \in [0, 1)$: the elementwise Pearson correlation coefficient between $\mathcal{G}_P$ and $\mathcal{G}_M$ and between $\mathcal{F}_P$ and $\mathcal{F}_M$. Given a parent, we draw mutants from this ensemble (while also preserving correlation κ between $\mathcal{G}_M$ and $\mathcal{F}_M$)—therefore the correlation between U_P and U_M is also ρ. Our main finding is that for ρ sufficiently far from 1, the eco-evolutionary phenomenology is similar to the independent invader limit of $\rho = 0$: this bolsters our confidence in basing qualitative conclusions on the case of independent invaders. We will more carefully define the evolutionary dynamics for correlated mutants in the simplified models that we introduce below, specifically in Section III C.

III. SIMPLIFIED MODELS

The saturation of the community-mean general fitness in the Red Queen eco-evolutionary steady state for $\kappa < 1$ is a particularly intriguing manifestation of continual evolution in an ecological system. We seek simpler—but still robust—models that display such a Red Queen steady state, but which allow us to separate out and independently tune the roles of ecological interactions and general fitnesses. The two related models that we shall study both have a generalized Lotka-Volterra form, but with different ensembles for the interaction matrix between strains. The first model is a linearized version of the CR model with the resource dynamics integrated out, yielding a maximum rank D for the strain interaction matrix. The second model is of a more standard Lotka-Volterra type, with direct interactions drawn from some ensemble and diagonal "niche" interactions enabling substantial diversity to coexist. For some ranges of parameters, both of these models exhibit a Red Queen phase characterized by constant turnover of biodiversity. In addition they allow us to isolate the effects of the general fitnesses on the eco-evolutionary dynamics, and study how the evolutionary dynamics depend on the width of the general fitness distribution.

In the cases where we find a Red Queen phase, the key quantities of interest are time-averaged observables in this nonequilibrium steady state: in particular the *diversity*, the *community-mean general fitness* and the *invasion probability* of new strains: we will use these quantities to characterize the Red Queen steady state that obtains.

A. Linearized model

In the Red Queen steady state of the CR model, the mean of $\sum_j \mathcal{F}_{j\alpha} n_j^*$ is large compared to its variations (Figure 14A), suggesting a self-consistent expansion in these variations. Such an expansion in the *differences* betweens strains yields general fitnesses at first order and interactions at second order (see Appendix C). In addition, the total population of the ecosystem $N = \sum_j n_j^*$ is roughly constant on evolutionary timescales (Figure 14B), due to the large mean of $\mathcal{G}$ and $\mathcal{F}$ relative to their variations. Therefore it is convenient to separate out the mean part of these matrices from their variations, and introduce zero-mean interaction matrices G and F. We additionally work in terms of fractional $\nu_i = n_i/N$, rather than absolute abundance, and integrate out the resource dynamics since these do not affect the fixed point. The simplified model that we introduce, and refer to hereafter as the *linearized model*, is

$$\frac{d\nu_i}{dt} = \nu_i \left(s_i + \sum_{\alpha=1}^{D} G_{i\alpha} R_\alpha - \Upsilon(t) \right) \tag{4a}$$

$$R_\alpha = -\sum_{j=1}^{S} F_{j\alpha}\nu_j. \tag{4b}$$

The term $\Upsilon(t)$ is a Lagrange multiplier, equal to $\sum_i \nu_i(s_i + \sum_\alpha G_{i\alpha}R_\alpha)$, which incorporates the average effects of

growth, death, and resource depletion, and keeps the population constant with $\sum_i \nu_i = 1$. Here, the per capita growth rate of each strain is a linear function of the abundances of all the other strains, with a quadratic part from Υ that is the same across all the strains, and an intrinsic general fitness given by s_i characterizing overall *selective differences* between strains: the s_i incorporate the parts of $\mathcal{G}_i$ parallel to the resource supply vector $\mathbf{K}$ in the CR model and play the role of the U_i. The resource vector $\mathbf{R}$ can have components which are negative since the mean of the F matrix is zero in the initially-assembled community—therefore $\mathbf{R}$ measures *deviations* of resource availability away from some positive mean. Viewing the linearized model as an expansion of the CR model, $\sum_j \mathcal{F}_{j\alpha} n_j^*$ has an $\mathcal{O}(D)$ mean and $\mathcal{O}(\sqrt{D})$ variations, and the general fitnesses come in at $\mathcal{O}(1/\sqrt{D})$ with interactions being $\mathcal{O}(1/D)$, as discussed in Appendix C.

The structure of Equation 4 is that of a generalized Lotka Volterra model or system of replicator equations (discussed further in Section III B), where the interaction matrix, denoted by V, has a structure inherited from the G and F matrices via $V = -GF^\intercal$, and G and F are $S \times D$ matrices. We take each element of G and F to be gaussian distributed with mean zero and unit variance, with no correlations within G or F. Elementwise correlations between G and F are again parameterized by $\kappa \in [0, 1]$ via $\mathrm{E}[G_{i\alpha} F_{j\beta}] = \kappa \delta_{ij} \delta_{\alpha\beta}$ with $\kappa \geq 0$ corresponding to the non-negative correlation between growth rates and consumption rates.

The off-diagonal entries of V have mean zero and standard deviation $\sqrt{D}$ while the diagonal entries have mean $-\kappa D$ and standard deviation $\sqrt{(1+\kappa^2)D}$. The parametrically-larger diagonal entries thus endow the interactions with a *niche* structure that stabilizes the dynamics. (Note that $\kappa < 0$ would result in unstable behavior with the diagonal entries of V having positive mean.) As in the CR model, the number of resources D sets the dimensionality of phenotype space, with the phenotype of strain i comprised of s_i along with the ith rows of G and F. The maximum number of coexisting strains at a stable fixed point of the linearized model is equal to D and will generally be less than—though proportional to—D.

When $\kappa = 1$, Υ is a convex Lyapunov function for Equation 4. If additionally $s_i = 0$, we have $\Upsilon = -\sum_\alpha (\sum_i G_{i\alpha} \nu_i)^2$ which is nonpositive. For nonzero s_i, the Lyapunov function gets an extra piece $\sum_i \nu_i s_i$ and can be of either sign, though it remains a convex function of the $\{\nu_i\}$.

For most of this paper, we will take the general fitnesses s_i to be drawn from a gaussian distribution $p(s)$ with mean 0 and variance Σ^2. In Section IV E we show that the value of Σ determines the early evolutionary behavior and the value of p_{inv} at steady state, with the shape of the large-s tail of $p(s)$ playing a controlling role. As the community evolves and the distribution of extant s_i pushes into the tail of $p(s)$, the effective Σ—the variance of the extant s_i—decreases. Therefore tuning Σ to be small *a priori* mimics the effects of *prior evolution* and allows us to study communities that have been evolving for a long time, without the long initial evolutionary transient.

As discussed previously in Section II B, for the CR model in Equation 1, the width of the U_i distribution is a factor of $\sqrt{D}$ larger than the width of the drive distribution. In the linearized model, this corresponds to $\Sigma = \mathcal{O}(\sqrt{D})$, since the distribution of the drives in a diverse community has $\mathcal{O}(\sqrt{D/L}) = \mathcal{O}(1)$ width. However, in the Red Queen steady state, as well shall see, the first and second order—in $1/\sqrt{D}$—components of the growth rate of each strain become comparable to one another. Thus we mostly consider $\Sigma = \mathcal{O}(1)$, and sometimes set $\Sigma = 0$, which shortens the transient period of evolution before the steady state is reached—and enables analysis—but does not change our conclusions. In Section IV E we also discuss non-gaussian distributions of the s_i, which affect quantitative properties but not the basic phenomenology.

B. Lotka Volterra model

In addition to the linearized model of Equation 4, we have studied the generalized Lotka Volterra (LV) model (or replicator equations) [41] which take the form

$$\frac{d\nu_i}{dt} = \nu_i \left(s_i + \sum_{j=1}^{S} V_{ij} \nu_j - \Upsilon(t) \right), \tag{5}$$

with $\Upsilon(t) = \sum_i \nu_i (s_i + \sum_j V_{ij} \nu_j)$. The LV model has similar structure to the linearized model of Section III A; the difference lies in the statistics and parameterization of the interaction matrix V. Instead of taking $V = -GF^\intercal$ with random G and F, in this LV model the V_{ij} are themselves gaussian random variables with $\mathrm{E}[V_{ij}] = -Q\delta_{ij}$, $\mathrm{E}[V_{ij}^2] = 1 + \gamma\delta_{ij}$, and $\mathrm{E}[V_{ij} V_{ji}] = \gamma$ for $i \neq j$. Here $\gamma \in [-1, 1]$ is the symmetry parameter tuning between predator-prey interactions for $\gamma < 0$ and competitive interactions for $\gamma > 0$: a rough correspondence for positive γ is $\gamma \sim \kappa^2$. The negative diagonal term $-Q$ is a "niche" parameter that measures the strength of self-interaction relative to inter-strain interaction—playing a similar role to $-\kappa\sqrt{D}$ in the linearized model. Our parameterization of the LV equations differs from another common parameterization in which interactions have nonzero mean [18], in that the V matrix captures *variations* in interaction magnitudes, with Υ taking the role of the mean interaction strength [22]. As in the linearized model, when the interactions are symmetric ($\gamma = 1$), Υ is a Lyapunov function of the dynamics, though in contrast to the linearized model [31], it can become a nonconvex function of the $\{\nu_i\}$ for large enough S [42].

The LV model has a similar ecological phase diagram to the CR model and linearized models, with a globally attracting fixed point of the dynamics when S is sufficiently small. The maximum L for a stable uninvadable fixed point scales as Q^2 with a γ-dependent coefficient [19]. Note that the scale of the drive distribution is $\mathcal{O}(1/\sqrt{L}) = \mathcal{O}(1/Q)$ in the LV model, as opposed to $\mathcal{O}(\sqrt{D/L}) = \mathcal{O}(1)$ in the linearized model, since the overall scale of the entries in the LV model smaller by a factor of $\sqrt{D}$ than in the linearized model.

In the LV model, unlike in the linearized and CR models, strains cannot be characterized by phenotypes. Although one can attempt to define a phenotype of strain i by s_i

along with its corresponding row and column of V, this phenotype depends on the rest of the community and thus changes—or grows in dimension—as the community turns over. Despite this difference in the mode of interaction between strains, the Red Queen phase that we find in the CR and linearized models also obtains for a broad range of parameters in the LV model, as discussed in Section III E.

C. Properties of invaders

Having defined the simplified ecological models of interest, we will now specify the evolutionary process. We first discuss general facts about invaders introduced to the community, and then define the specific parameterization of invaders that we have used for our simulations.

As in the CR model, whether a new strain successfully invades the extant community or not is determined by its invasion fitness or bias, now written as $\xi_i = s_i + \zeta_i - \Upsilon$ with $\zeta_i = \sum_j V_{ij}\nu_j$ in the LV model and $\zeta_i = -\sum_\alpha G_{i\alpha}R_\alpha$ in the linearized model. Splitting the bias up into the general fitness piece s_i, the Lagrange multiplier Υ and the drive ζ_i is useful since it separates the intrinsic and extrinsic contributions to the bias. Strains with positive bias can invade the community and stabilize with abundance proportional to their bias, whereas strains with negative bias go extinct. As in the CR model, when running our simulations, we sample properties of the invader a conditional upon $\xi_a > 0$ [40]. Strain extinction occurs when the bias of a strain goes negative, or equivalently, its abundance goes to 0 in the ecological dynamics.

We first consider evolution in the LV model in which new invaders are independent of the properties of extant strains; their invasion probability is therefore $p_{inv} = 1 - \Phi[\Upsilon/\sqrt{\sum_i \nu_i^2 + \Sigma^2}]$ where Φ is the standard normal CDF. An invader strain a is generated by drawing a new row and column of V from the original gaussian ensemble with $\mathrm{Corr}[V_{ai}, V_{ja}] = \gamma\delta_{ij}$. The general fitness s_a is chosen independently from a gaussian with mean 0 and variance Σ^2. In the LV model, the lack of phenotypes makes attempts to parameterize correlations between parent and mutants *ad hoc* for general γ [37]. Therefore we confine our study of the LV model to the case of independent invaders, which nonetheless will be particularly useful for gaining analytical understanding.

In models with phenotypes, such as the CR or linearized model, there is a natural way to generate mutants through small changes to the phenotype of an extant parent strain. This procedure creates a mutant whose interactions with all other strains are similar to those of its parent. In our gaussian ensemble, the probability of any parent generating a mutant that can invade is the same—therefore we can, in an unbiased way, simply select a parent with probability proportional to its abundance.

The parameter $\rho \in [0, 1)$ describes the correlation between parent P and mutant M. The mutant phenotype is drawn from an ensemble that preserves $\mathrm{E}[G_{M\alpha}G_{P\beta}] = \mathrm{E}[F_{M\alpha}F_{P\beta}] = \rho\delta_{\alpha\beta}$, $\mathrm{E}[G_{M\alpha}F_{M\beta}] = \kappa\delta_{\alpha\beta}$, and $\mathrm{Corr}[s_M, s_P] = \rho$. We fix the desired correlations by

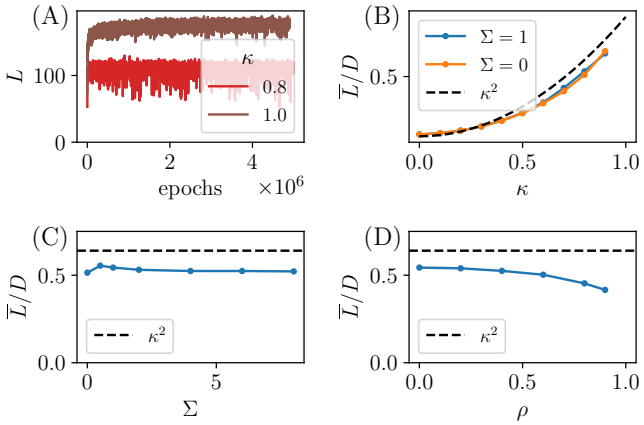

Figure 4. Steady-state community size, $\overline{L}$, in linearized model as function of various parameters. Default values $D = 200$, $\kappa = 0.8$, parent-mutant correlation $\rho = 0$, width of distribution of selective differences $\Sigma = 1$, but each varied as specified per panel. A) L over evolutionary time for $\kappa = 0.8, 1$. Although L appears to be reaching steady state for both parameters, for $\kappa = 1$, Υ and p_{inv} indicate it is not (Figures 5 and 6). (B) $\overline{L}$ as a function of κ, for $\Sigma = 0$ and 1. Dotted line shows maximum diversity in *top-down assembled* community; in evolved Red Queen phase diversity is lower. (For $\Sigma = 1$ $\kappa = 0.9$, steady state not quite reached and $\overline{L}$ underestimated). (C) $\overline{L}$ depends only weakly on Σ (D) Dependence on mutant-parent correlations: For ρ not too near unity $\overline{L}$ is weakly dependent on ρ.

drawing the phenotype of M as

$$G_{M\alpha} = \rho G_{P\alpha} + \sqrt{1-\rho^2}Z_\alpha \tag{6a}$$

$$F_{M\alpha} = \rho F_{P\alpha} + \sqrt{1-\rho^2}(\kappa Z_\alpha + \sqrt{1-\kappa^2}Z'_\alpha), \tag{6b}$$

$$s_M = \rho s_P + \sqrt{1-\rho^2}\Sigma Z'' \tag{6c}$$

where the $\{Z_\alpha\}$, $\{Z'_\alpha\}$ and Z'' are uncorrelated standard normal random variables. This choice ensures that the elements of the interaction matrix $V = -GF^\intercal$ have correlations $\mathrm{Corr}[V_{Mi}, V_{Pj}] = \mathrm{Corr}[V_{iM}V_{jP}] = \rho\delta_{ij}$ for $i, j \notin \{M, P\}$. The invasion probability of a mutant drawn from this ensemble is given by

$$p_{inv} = 1 - \Phi\left[\sqrt{\frac{1-\rho}{1+\rho}}\frac{\Upsilon}{\sqrt{|\mathbf{R}|^2 + \Sigma^2}}\right] \tag{7}$$

where Φ is the standard normal CDF. In this paper we restrict study to large effect mutations, with ρ such that $\sqrt{1-\rho^2} = \mathcal{O}(1)$. The behavior as $\rho \to 1$—small effect mutations—is both interesting and biologically relevant, and we will discuss it in depth in future work.

D. Evolution in the linearized model

The motivation for introducing the linearized model is to capture the phenomenology of the CR model—continual turnover without ever-increasing general fitness—in a simple setting where the effects of the general fitnesses can be separated out from the interactions, and with a shorter transient period before the steady state is reached. We begin by describing the basic phenomenology of evolution in

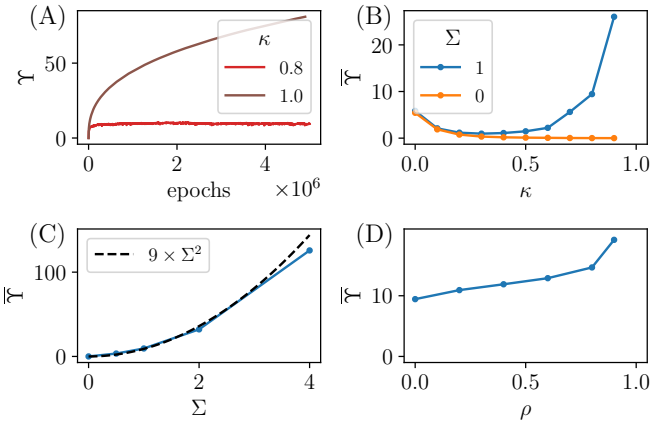

Figure 5. Steady-state Lagrange multiplier $\overline{\Upsilon}$—loosely community "fitness"— as a function of parameters. (A) For $\kappa = 1$, Υ (Lyapunov function in this case) is ever-increasing. For $\kappa = 0.8$ it reaches steady state. (B)–(D) Dependence of $\overline{\Upsilon}$ on κ, Σ and ρ. (B) $\overline{\Upsilon}$ as function of κ. For $\Sigma = 0$ the elements of growth and feeding vectors of strains, G and F, do not push into tails of their distribution. Simulations are less reliable for small κ (see Appendix D). (C) Dotted line for $\overline{\Upsilon}$ as function of Σ is rough fit to predicted form, $\overline{\Upsilon} \sim \Sigma^2$. At $\Sigma = 4$, Υ has not yet saturated. Default parameters same as in Figure 4.

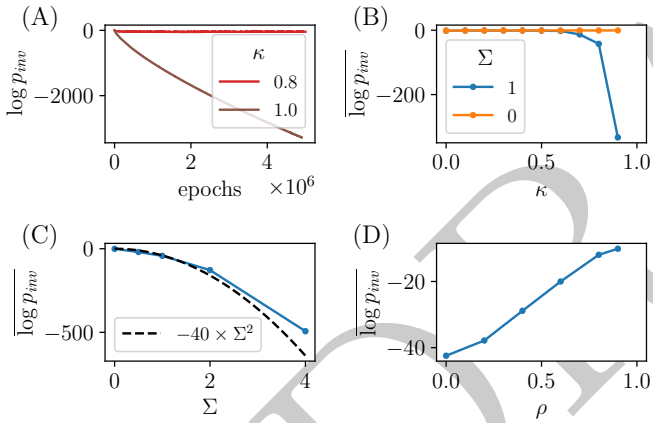

Figure 6. Steady-state log invasion probability $\overline{\log p_{inv}}$ as a function of parameters (A) Invasion probability continues to decrease for $\kappa = 1$ but reaches steady state for $\kappa = 0.8$. (B)–(D) Dependence of $\overline{\log p_{inv}}$ on κ, Σ and ρ. Although $\overline{\log p_{inv}}$ systematically underestimates $\log \overline{p_{inv}}$, the difference is not important for our purposes here. The dashed line for $\overline{\log p_{inv}}$ as a function of Σ is a rough fit to the theoretical dependence $-\log \overline{p_{inv}} \sim \Sigma^2$, expected from the assembled community (Equation 8b). As in Figure 5, the simulations for $\Sigma = 4$ have not reached steady state and $\overline{\log p_{inv}}$ is overestimated. Parameters are the same as in Figure 4.

the linearized model of Equation 4, with the evolutionary dynamics of Equation 6. In general, the evolutionary dynamics of the model are parameterized by D, κ, ρ and Σ, while the initial condition requires us also to specify the size of the initial pool of strains, S. However S only plays a role in the transient behavior, and we are most interested in the Red Queen phase itself. To show convergence to the same phase from different initial conditions, we will consider starting both from a large-S assembled community, and from the smallest, $S = 1$.

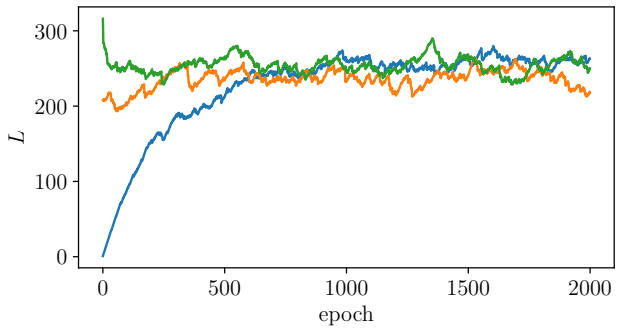

Figure 7. The same steady state is reached over a range of initial community sizes S in the LV model with independent invaders. All initial conditions tending toward the same Red Queen phase after a short initial transient. Here $\gamma = 0$, $Q = 20$ and $\Sigma = 0$.

In the Red Queen state, key quantities are $\overline{L}$, $\overline{\Upsilon}$ and $\overline{p_{inv}}$, where we denote averages over evolutionary time with an overbar. In Figure 4A we plot the dependence of L on evolutionary time for two values of κ: 0.8 and 1. There is a transient during which the diversity builds up, after which both trajectories flatten out. Figure 5A shows that for $\kappa = 0.8$ there is a Red Queen steady state with roughly constant Υ—indicating that p_{inv} should saturate. However for $\kappa = 1$, L continues to increase more and more slowly and there is no Red Queen phase as Υ continues to increase.

We have looked at the quantities L, Υ and p_{inv} for a range of parameters κ, Σ and ρ. Figures 4, 5 and 6 show that the eco-evolutionary dynamics is similar across across a range of ρ, Σ, and κ. The important conclusion from these simulations is that the Red Queen phase obtains across a range of parameters for $\kappa < 1$, and that parameter choices, though affecting the length of the transient before the steady state, do not eliminate the Red Queen phase. Therefore we should be able to gain insight into the Red Queen state by studying just a few values of the relevant parameters. The value of D sets the overall scale of L but, as long as it is large, does not matter much—we therefore choose a large $D = 200$ and $\kappa = 0.8$ for our simulations. This choice yields a large number (roughly $D/2$) strains surviving in the Red Queen and phase and keeps away from the non-generic $\kappa = 1$ behavior.

In Figure 4A , the observed $\overline{L}$ is compared with the curve $\kappa^2 D$ which is the maximum L in a top-down assembled community with $\mathcal{G}$ and $\mathcal{F}$ drawn from the gaussian ensemble for the linearized model (Appendix G). We see that the realized $\overline{L}$ from simulations is less than this upper bound, which, although it is not a strict bound, we will rationalize in Section IV B. More importantly, in Section IV E we give scaling arguments for how $\overline{\Upsilon}$ and $\log \overline{p_{inv}}$ at steady state depend on κ and Σ: these scalings are compared with numerical data in Figures 5 and 6.

E. Evolution in the LV model

Given the apparent similarities between the CR and linearized models, it is natural to ask how the eco-evolutionary

phenomenology in the LV model resembles or differs from these cases. We have investigated evolution (with $\rho = 0$) in the LV model across a range of γ and Q, the symmetry and niche parameters defined in Section III B. For a range of γ we find a Red Queen phase analogous to those of the CR and linearized model, with the product of Q^2 and a function of γ determining the number of strains in the steady state. Similarly to in the linearized model, L in the Red Queen phase fluctuates around a mean value $\overline{L}$ that is less than the maximum L from a top-down assembled community. The gap between the realized $\overline{L}$ and the assembled upper bound as a function of γ is shown in Figure 15A. This gap diverges as $\gamma \to -1$, meaning that in this regime, the Red Queen steady state is much less diverse that the largest possible community assembled top-down. In contrast, in the linearized model, this gap is bounded and does not grow large—however there is no regime of the linearized model that corresponds to the negative cross-diagonal correlations in V that characterize the LV model with negative γ.

The fact that the top-down assembled community can be substantially larger than the evolved community in the LV model allows us to check that the Red Queen phase obtains across a range of initial number of strains S. In particular, since the top-down assembled community can have $L > \overline{L}$, there are situations in which there is a naturally-findable stable ecological community that is somewhat unstable to evolution, with L decreasing as the evolving community converges to the Red Queen phase. Figure 7 shows this behavior in the LV model for $\gamma = 0$ and $\Sigma = 0$, with L approaching $\overline{L}$ from both above or below, depending on the S of the initial community. Note that this means that even in simple models the question of whether evolution increases or decreases diversity from a top-down assembled initial condition has no general answer [27].

Although we find a robust Red Queen phase for a range of γ and Σ in the LV model, closer investigation of the effect of γ reveals an interesting feature. The evolutionary dynamics in the LV model change sharply with γ, appearing to exhibit a discontinuous transition around $\gamma_c \approx 0.65$ for $\Sigma = 0$. For $\gamma < \gamma_c$ a Red Queen phase obtains, while for $\gamma > \gamma_c$ we find a phase in which the rate of successful invasion is ever-slowing and a few strains rise to high abundance. We therefore name this phase the "oligarch" phase of eco-evolutionary dynamics—a counterpart to the Red Queen.

In contrast to the LV model, the eco-evolutionary Red Queen steady state of the linearized model appears to obtain for all $\kappa < 1$, with $\overline{\Upsilon}$ diverging as κ approaches 1 and evolutionary transients correspondingly lengthening (Figure 5B). We expect similar behavior of $\overline{\langle U \rangle}$ diverging with $\kappa \to 1$ in the CR model. We discuss the oligarch phase in greater detail in Section V, and leave its fuller analysis for future work. For now we emphasize that this striking difference in phenomenology between models shows the possibility of multiple distinct eco-evolutionary phases, each robust over a range of parameters.

IV. ANALYSIS

In order to understand the phenomenology of the Red Queen phase described above, we first discuss the *top-down assembled* community of the linearized model in which all strains are brought together at once, and change in time according to their ecological interactions. An understanding of the ecological phase diagram in this setting is informative for analyzing the Red Queen phase, and gives us an idea of how $\overline{\Upsilon}$ and $\overline{p_{inv}}$ scale with the parameters in the Red Queen phase.

We then introduce a particular limit of the linearized model which reduces to the LV model with $\gamma = 0$. With the further simplification of $\Sigma = 0$—yielding the simplest ensemble of the LV model—we can exactly solve for the steady state of the evolutionary dynamics in the limit of large diversity. Key quantities are the distribution of strain abundances in an evolved community—strikingly different than a top-down assembled community—and temporal correlation functions of strain abundances in evolutionary time.

Last, we consider the effects of selective differences, presenting general scaling arguments for the dependence of $\overline{L}$, $\overline{\Upsilon}$ and $\overline{p_{inv}}$ on Σ, which agree with the intuition gleaned from the assembled communities. We generalize to different distributions, $p(s)$, and show how the primary pathologies of the gaussian distribution can be alleviated.

A. Assembled communites

In a top-down assembled community of the linearized model, all the strains are initialized at positive abundance, and are governed by the deterministic dynamics of Equation 4 without a sharp extinction cutoff. The cavity method can be used to analyze the assembled community with S strains in total and D resources, in the limit of large S and D with the ratio S/D constant. The spirit of the cavity method is to consider a large community to which one adds one new strain and one new resource: these each act as small perturbations to the community. The abundance of the new strain is then determined by its invasion fitness, modified by the community-wide response to its introduction, and the new resource is treated similarly. One then enforces self-consistency conditions that the statistics of the strains and resources in the community are the same as the statistics of the newly added strain and resource. These conditions rely on the community being assembled with independent interactions—since then the independently-drawn invading strain and resource are from the same ensemble as the rest of the community. By solving the self-consistency equations one can extract abundance distributions of ν_i and R_α, and solve for L/D and Υ as a function of S/D, κ and Σ. Similar results can be obtained for the non-linear CR model [32] and—more simply—the LV model [19].

Details of the cavity analysis are in Appendix G. The main result is that generically the linearized model exhibits two phases as a function of the ratio S/D. For $\Sigma > 0$, when S/D is small enough, there is a stable globally attracting fixed point, uninvadable by the strains that are going extinct: this fixed point is described by the cavity solution

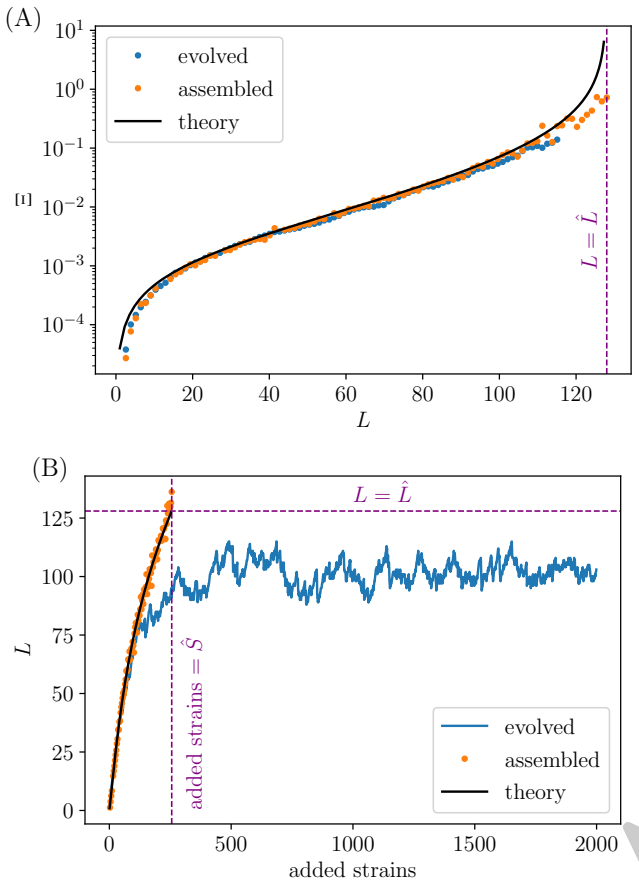

Figure 8. The stability to evolutionary perturbations differs between top-down *assembled* and *evolved* (or bottom-up assembled) communities. (A) The fragility Ξ, a community-wide measure of susceptibility to a global perturbation, as a function of the number of extant strains. In the assembled community, this quantity diverges at the transition between stable and unstable phases (denoted by the vertical dashed line). The theory curve is for a top-down assembled community. (B) The number of surviving strains at the fixed point is lower than the saturated diversity $\hat{L}$, indicated by the horizontal dashed line. The vertical dashed line indicates $\hat{S} = 2\kappa^2 D$, which is the number of starting strains needed to saturate the diversity. The x axis, "added strains," represents epochs for the evolved curve and S for the assembled curve. The theoretical result is shown for a top-down assembled community. Parameters are $\kappa = 0.8$, $D = 200$, and $\Sigma = 0$.

and has $L/D < \kappa^2$. The abundances of the strains in the stable community are distributed as a truncated gaussian so that there are strains with arbitrarily small abundances, indeed there is a constant density of abundances at zero as seen in Figure 10. Concomitantly, the strains destined for extinction have negative invasion fitnesses with a distribution that has a constant density of states near zero. Thus the assembled community has many close-to-marginal strains.

When the initially assembled diversity, S, becomes larger than a (Σ-dependent) critical value $\hat{S}$, at which $L = \kappa^2 D$, the cavity solution becomes unstable and chaotic dynamics or multi-stability may ensue [20]. We use a hat to denote the values of quantities at this phase transition, and refer to the community at this transition point as "saturated."

The number of initial strains, $\hat{S}$, needed to achieve this saturated state, diverges as $\kappa \to 1$ as long as $\Sigma > 0$—therefore for $\kappa = 1$ and $\Sigma > 0$ the cavity solution is always stable. When $\Sigma = 0$ the picture for $\kappa < 1$ remains the same, while at $\kappa = 1$ there is a transition (for $S > 2D$) to a nongeneric "shielded" phase [31] in which $L/D = 1$—the maximum allowed by competitive exclusion—and the state is highly marginal.

With an extinction threshold, even for $S > \hat{S}$ the ecological dynamics will generally reach a stable fixed point with $L \approx \kappa^2 D$. However the resulting community will generally be unstable to re-invasion by some of the strains that had gone extinct. Furthermore, in this super-saturated regime there are multiple possible stable communities, almost all of them invadable by some of the extinct strains. Which one occurs will thus depend on the initial conditions. The question of whether or not stable uninvadable communities are likely to exist for large D is unresolved except for the special $\kappa = 1$ case for which there is an absolute maximum of the Lyapunov function. However it is believed that even if such fixed points exist for $\kappa < 1$, they may attract only an exponentially small fraction of initial conditions.

We can glean insights about the properties of an evolved community with $\rho = 0$ from an analysis of the near-saturated assembled community, since after long period of evolution, a large number of strains—many more than $\hat{S}$—will have had a chance to invade the evolved community. Naively, one might think that the end result is similar to assembling the whole community at once. However as we shall see, the evolved community never becomes saturated in the way that the assembled community can be.

As we would like to understand behavior for Σ large compared to 1, which is what occurs "naturally" (e.g. from the CR model), we focus for now on this limit. In the linearized model the saturated assembled community has $\hat{L} = \kappa^2 D$ for all Σ and, for $\Sigma \gg 1$,

$$\hat{\Upsilon} \approx \frac{\Sigma^2 \kappa}{1 - \kappa^2} \tag{8a}$$

$$\hat{S} \sim \exp\left[\frac{\kappa^2 \Sigma^2}{2(1-\kappa^2)^2}\right]. \tag{8b}$$

The reciprocal of $\hat{S}$ scales with the fraction of surviving strains, and therefore the invasion probability of a single independent invader is of order $D/\hat{S}$.

We conjecture that the forms of the scalings of $\hat{\Upsilon}$ and $\log \hat{S}$ with Σ in the assembled community also describe the time-averaged quantities in the Red Queen steady state, i.e. that $\overline{\Upsilon} \sim \hat{\Upsilon}$ and $\log \overline{p_{inv}} \sim -\log \hat{S}$, albeit with unknown coefficients. The scalings in Equation 8, along with the guess that $\overline{L} \sim \hat{L}$, motivate the theory curves in Figures 4, 5 and 6: these are consistent with numerical data from the Red Queen phase. In Section IV E we give an argument that these scalings of $\overline{\Upsilon}$ and $\overline{p_{inv}}$ with Σ should be expected on evolutionary grounds.

B. Fragility of communities

In the eco-evolutionary Red Queen phase, ecological communities remain stable, but are different from top-down assembled communities since their interaction statistics are

conditioned on evolution and, crucially, they would be *unstable to invasion* by some fraction of previously invaded strains that have gone extinct. An indication of this distinction, shown in Figure 4, is the diversity of the Red Queen phase: $\overline{L}$ is smaller than in saturated assembled communities, $\overline{L} < \hat{L} = \kappa^2 D$, across the range of κ. When a community is assembled one strain at a time with *permanent* extinctions, it is not possible to reach as high diversity as reached by top-down assembly. What is responsible for this gap between $\overline{L}$ in the Red Queen phase and $\hat{L}$ from the saturated assembled community? The answer is associated with the relative fragility of the two states.

The transition between phases in the assembled community is marked by the onset of an instability in the cavity solution. This instability entails the divergence of a community-level property that we call the *fragility* and denote by Ξ. The fragility quantifies the variance of the changes in strain abundances in response to a random perturbation to the growth rates of all the strains. Concretely, if for each strain i we add a small independently random term h_i to its bias, with $\mathrm{E}[h_i] = 0$ and variance $\mathrm{E}[h_i^2]$, (loosely like applying random fields) the fragility is defined by $\sum_i \mathrm{E}[\delta\nu_i^2] = \Xi \times \mathrm{E}[h_i^2]$. The fragility can also be written as $\Xi = \sum_i X_{ii}^2 \times \mathrm{Tr}[X^\intercal X]$ where the $X_{ij} = \frac{d\nu_i}{d\xi_j}$ are elements of the susceptibility matrix X of the community. Deep in the stable phase the fragility is small, as small perturbations to strain growth rates do not cause abundances to reshuffle by much. However as the transition is approached and L nears $\kappa^2 D$, the fragility diverges, indicating a breakdown in the stability of the cavity solution.

The evolutionary dynamics can be understood by considering the effects of a new successfully invaded strain on those already in the community. A new strain adds a small random part to the biases of the other strains. For an independent invader a which reaches a stable abundance ν_a, its contribution to the bias of another strain, i, is $V_{ia}\nu_a$. The variance of this random perturbation is $\mathrm{Var}[V_{ia}\nu_a] = \nu_a^2 D$ for the linearized model. This is multiplied by a factor of $\Xi/L \sim 1/L^2$ to yield $\mathrm{Var}[\delta\nu_i]$ of order $1/L^3$ and therefore $\delta\nu \sim L^{-3/2}$. For a typical strain with $\nu \sim 1/L$, this perturbation will be small. However in a top-down assembled community, the lowest abundance strains will have ν smaller than typical by a factor of $1/L$, and $\mathcal{O}(\sqrt{L})$ of these will have abundance less than the magnitude of the perturbation. This implies that the invasion will drive the bias of $\mathcal{O}(\sqrt{L})$ of the lowest abundance strains negative and out of the community. Concomitantly, if we do not enforce permanent extinctions, the perturbation will increase the bias of a similar number of barely-extinct strains and these will enter the community. As long as Ξ is not large, this number of extinctions and invasions will be small. As $S \nearrow \hat{S}$, Ξ diverges and the assembled community will be shaken a lot by a single additional strain.

The behavior of an *evolving* community—with permanent extinctions—in response to a small random perturbation is quite different. When the community has just been assembled, if it is close to saturated, then a fraction of the strains with $\nu \leq \mathcal{O}(L^{-3/2})$ will go extinct. Under the perturbations from further invasions, the density of low abundance strains will be hollowed out by this diffusion-like process with an absorbing boundary condition at zero, resulting in a density that goes linearly to zero as $\nu \to 0$ (see Figure 10). The diffusion coefficient of abundances in evolutionary time is proportional to the fragility of the community, so if Ξ is large, then the perturbations are amplified and more extinctions result, on average, from each successful invader. As the diversity grows, we expect that (as in the top-down assembled communities), the fragility also grows. When it is large enough that on average one extinction is driven by each invasion, the diversity stabilizes. This must thus occur while the fragility is not too large suggesting—although not implying because of the complexities on conditioning on the evolutionary history—that the Red Queen state will be less diverse than the maximal assembled diversity, as observed in Figure 8B. The ratio $\overline{L}/\kappa^2 D$ depends on the value of κ; this is presumably due to the dependence of Ξ on κ. (We observed a similar difference between assembled and evolved communities in our previous work on evolving spatiotemporally chaotic communities [37].)

For the LV model with $\gamma = 0$, the fragility can be calculated simply. For each strain with positive bias, $\nu_i = \xi_i/Q$ and so the susceptibility to an additional growth rate, h_i, is $d\nu_i/dh_i = d\nu_i/d\xi_i = 1/Q$. However the change in each ν_i causes a small random change of the drive of all the other strains, which increases the effective variance of the random field, and so on. Summing up these effects yields a total effect of random h_j's given by $\sum_i (\delta\nu_i)^2 = \Xi\,\mathrm{Var}[h_j]$ with the fragility $\Xi = \frac{L/Q^2}{1-L/Q^2} = \frac{L}{Q^2-L}$. This result does not depend on how the community is formed nor on the selective differences if they are present. It shows right away the maximum size of a stable community is $\hat{L} = Q^2$ which is reached for an assembled community. For the evolved community, Ξ cannot be large, implying that $\overline{L} < \hat{L}$.

In recent work, de Pirey and Bunin [43] have observed and studied a similar phenomenon of depletion of low-abundance strains due to continual perturbations to the community caused by invading strains. These authors looked at purely *ecological* model with small migration from a mainland that prevents total extinction of any strain—here species jumping up from the brink of extinction play the role of invaders in our evolutionary model. The similarities between this ecological model and our work are discussed in Appendix L; in the evolutionary problem we study, more analytical progress can be made given the simplicity of the extinction boundary condition in contrast to the boundary condition at zero abundance that arises from migration. In particular, with the migration-induced boundary condition, the steady state distribution of ν does not vanish as $\nu \to 0$ and the boundary condition must be determined self-consistently from the ecological dynamics.

C. Exact solution in simple case

Having understood some features of the eco-evolutionary phenomenology by comparison with the saturated assembled community, we now proceed to directly analyze the evolutionary dynamics for a particularly simple choice of parameters.

With $\kappa > 0$, there are correlations κ^2 between the cross-diagonal elements of the interaction matrix V, as in the

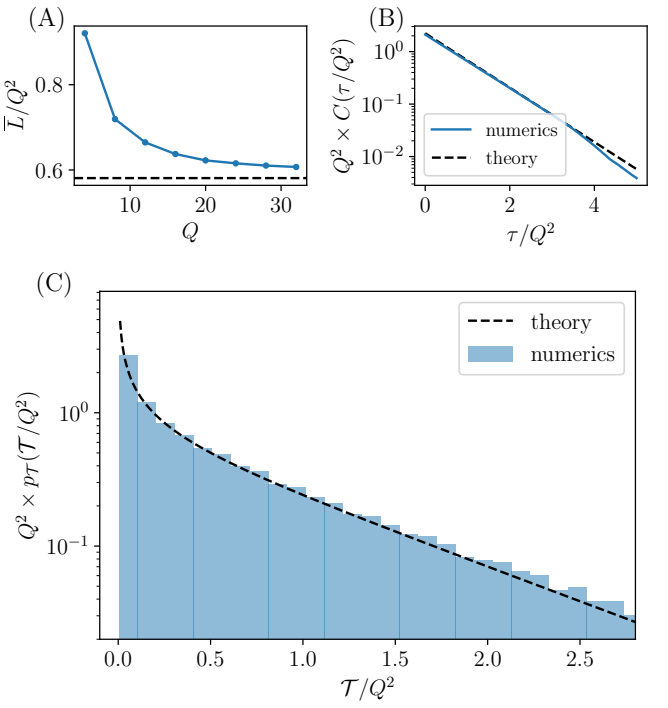

Figure 9. Results of the evolutionary cavity calculation agree with numerics for $\gamma = 0$ LV model with independent invaders. (A) The number of strains in the Red Queen steady state converges to $\overline{L} \approx 0.58 \times Q^2$ (the dotted black line) as $Q \to \infty$, in agreement with theory (Equation 13). (B) The correlation function $C(\tau) = \sum_j \nu_j(T)\nu_j(T+\tau)$ agrees with the theoretical prediction of Equation 12 without any fit parameters. (C) The distribution of strain lifetimes $\mathcal{T}$ in the steady state, normalized by the basic timescale Q^2. There is good agreement with the theoretical prediction of Equation 14. $\gamma = 0$, $\Sigma = 0$, $Q = 20$ in all panels unless otherwise noted.

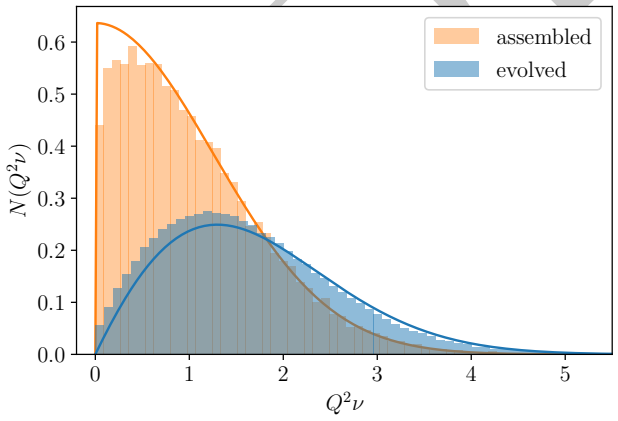

Figure 10. The number density of the scaled abundance $z = Q^2\nu$ in both a saturated assembled community and the evolved Red Queen steady state, with normalization $\int dz N(z) = \overline{L}/Q^2$. Histograms are numerical data and solid lines are analytical curves from a cavity calculation in the top-down assembled case and the solution to Equation J12 in the evolved (bottom-up assembled) case. $\gamma = 0$, $Q = 20$, $\Sigma = 0$.

case of $\gamma > 0$ for the LV model. These correlations induce complex memory into the evolutionary dynamics since the effect of an invader a on a strain i in the community via V_{ia} feeds back via V_{ai} onto a. This feedback on a is coherent across the extant strains with magnitude proportional to κ^2 (or γ). Thus the properties of a strain in the community depend on its effects on the other strains over all the epochs since its invasion—in particular on its abundance in these earlier epochs. This effect makes the evolutionary dynamics difficult to analyze, as the form of this memory kernel needs to be self-consistently determined along with the dynamics of the strains abundances in evolutionary time: we set this analysis up in Section IV D but do not carry it through.

However, there is a limit of the linearized model that is simple: if we take $D \to \infty$ and $\kappa \to 0$ while keeping the product $\kappa^2 D$ finite, we can rescale the interaction matrix by a factor of $\sqrt{D}$ to obtain the LV model with $\gamma = 0$ and $Q = \kappa\sqrt{D}$, expecting $\overline{L} = \mathcal{O}(Q^2)$ in the Red Queen phase. (Note that in this limit, the elements of V become gaussian.) The fact that for $\gamma = 0$ the interaction matrix V has no correlations across the diagonal makes the feedback effects smaller by a factor of $1/\sqrt{L}$ (and of random sign) and hence negligible—therefore the analysis that we undertake becomes tractable. We first treat the case of $\gamma = 0$, $\Sigma = 0$, and then set up the general structure of the cavity calculation for nonzero γ and Σ, before describing heuristically the effects of $\Sigma > 0$.

Our analysis of the Red Queen phase proceeds by means of a dynamical cavity method, which is one way of carrying out dynamical mean-field theory (DMFT) as used in systems with quenched randomness. The idea is to consider the evolutionary-time dynamics of a focal "cavity strain" labelled 0, that could potentially enter the community, persist for some number of epochs, and later go extinct. For $\gamma = 0$, the abundance of the cavity strain while it is in the community is determined by its bias, if positive. In this simple case its dominant interactions are with itself so that $\nu_0 = \xi_0/Q$ in the limit of large L. However the bias, $\xi_0(T) = s_0 + \zeta_0(T) - \Upsilon(T)$, changes in evolutionary time, T. If the strain attempts to invade at time $\mathbb{T}_0$, then its abundance in the community at all later times is

$$\nu_0(T) = \frac{\xi_0(T)}{Q} \mathbb{1}\left[\xi(T') > 0 \;\forall\; T' \in (\mathbb{T}_0, T)\right] \qquad (9)$$

where $\mathbb{1}[E]$ is the indicator function which is unity when event E occurs and zero otherwise. The cavity strain's abundance is only nonzero as long as its bias remains positive—and it goes irrevocably extinct once its bias goes negative. Therefore the statistics of the cavity strain abundance are determined by the statistics of its bias, conditional on non-extinction.

To carry out the cavity analysis, one needs to make an *Ansatz* for the statistics of the cavity bias, and then carry out the conditioning on survival explicitly to get the dynamics of the cavity strain's abundance. One then enforces self consistency, which relates the survival-conditioned dynamics of strain abundances in the community to the statistics of the unconditioned cavity bias. This is possible since the cavity drive is simply $\zeta_0(T) = \sum_{j \in \mathcal{C}(T)} V_{0j}\nu_j(T)$, which has gaussian correlations for large L. Since the V_{0j} are independent and not conditioned on properties of the com-

munity, we have simply

$$C(\tau) \equiv \overline{\zeta_0(T)\zeta_0(T+\tau)} = \sum_j \overline{\nu_j(T)\nu_j(T+\tau)} \qquad (10)$$

where the sum is over *all* strains that have invaded before time T—most of which will be extinct at T or $T+\tau$ and therefore not contribute to the correlation function. For large $\overline{L}$, the average over T, denoted by the overbar, is not needed: we expect $C(\tau)$ to be "self-averaging" and depend only on the time-difference τ (up to subdominant corrections).

The self-consistency condition at the heart of the cavity method is that the autocorrelation of the cavity strain, averaged over s_0, $\zeta_0(\mathbb{T}_0)$, and invasion time $\mathbb{T}_0$, is the same as the autocorrelation function of each of the strains that determine $C(\tau)$ via Equation 10. $\overline{\Upsilon}$ has to be adjusted to achieve this self-consistency (just as Υ is determined for the static ecological cavity analysis of Appendix G).

We now specialize to the simplest case where all s_i are zero. Simulations of the $\gamma = 0$, $\Sigma = 0$ Lotka Volterra model (Figure 15B) suggest that in this case $\overline{\Upsilon} = 0$ and we make the *Ansatz* that this is exact. Hoping for some luck, we then make the simplest possible *Ansatz* for the statistics of $\zeta_0(T)$: namely that it has an exponentially decaying correlation function $C(\tau) = \sqrt{J/b} \times e^{-b\tau}$. $C(0)$ determines the unconditioned distribution of the cavity drive—including at $\mathbb{T}_0$, the time of its invasion. This *Ansatz* can be translated into a stochastic process that determines ζ_0:

$$\frac{d\zeta}{dT} = -b\zeta + \sqrt{2J}\eta(T) \qquad (11)$$

with T the time measured in epochs and $\eta(T)$ white noise satisfying $\langle \eta(T)\eta(T')\rangle = \delta(T-T')$ (angular brackets denoting averages over the stochasticity). The white noise represents the effects of adding independent invaders which cause the diffusive effects discussed in Section IV B, and the deterministic term is, roughly, regression to the mean ζ of zero, and can be seen to arise from the correlation between ζ and $\delta\zeta$ due to the same elements of V appearing in both quantities [37]. We have dropped strain indices here because there are no selective differences and we are operating under the cavity hypothesis that all strains are statistically equivalent. The quantities b and J are (for now) phenomenological parameters that must be fixed by self-consistency. The advantage of having an effective stochastic differential equation for ζ, along with $\overline{\Upsilon} = 0$, is that the method of images can be used to condition upon $\zeta > 0$ from the time of its invasion until the time of interest.

In order to calculate the right hand side of the self-consistency condition Equation 10, we first need to calculate the two-time correlation function $\langle \nu(T)\nu(T+\tau)\rangle$ averaged over the stochasticity in Equation 11. $\nu(T)$ is given by Equation 9 with $\xi(T) = \zeta(T)$ since $s = \overline{\Upsilon} = 0$, and we assume that the strain successfully invaded the community at some initial abundance, $\nu(\mathbb{T})$ at its invasion time $\mathbb{T}$. From our *Ansatz*, this initial $\nu(\mathbb{T})$ is distributed as a gaussian random variable with standard deviation $\frac{1}{Q}\sqrt{J/b}$, truncated below zero. In order to calculate $C(\tau)$ from the strains in the community, we integrate $\langle \nu(T)\nu(T+\tau)\rangle$ over all initial times $\mathbb{T}$—equivalent to fixing $\mathbb{T} = 0$ and integrating over all T—and over all starting abundances $\nu(\mathbb{T})$ weighted by the truncated gaussian measure.

A self-consistent solution is possible if the result of this calculation gives an exponentially decaying correlation function with the same amplitude and timescale as the correlation function of the cavity drive $C(\tau) = \sqrt{J/b} \times e^{-b\tau}$. Fortunately, this turns out to be the case. An additional self-consistency condition fixes $\sum_i \nu_i = 1$. Put together, these conditions allow us to solve for J and b. We then compute the diversity $\overline{L} = \sum_i \Theta(\nu_i)$. These calculations are carried out in Appendix J. The key result is the self-consistent exponential solution for the correlation function

$$C(\tau) = \frac{2\pi}{Q^2}\left(\frac{1+2\log 2}{4}\right)^2 \exp\left[-\frac{1+2\log 2}{2Q^2}\tau\right], \qquad (12)$$

and

$$\overline{L} = \frac{2\log 2}{1+2\log 2}Q^2 \approx 0.58 \times Q^2. \qquad (13)$$

The timescale of the decay of the correlation function is $\mathcal{O}(Q^2) = \mathcal{O}(\overline{L})$, consistent with the community turning over every $\mathcal{O}(\overline{L})$ successful invasions.

Figure 9 compares these analytical results to numerics on the $\gamma = 0$, $\Sigma = 0$ LV model. As Q increases in Figure 9A, the numerics get closer to the large-$\overline{L}$ regime in which the theory holds, and $\overline{L}/Q^2$ in steady state approaches $\frac{2\log 2}{1+2\log 2}$ from above. Figure 9B shows the scaled correlation function $Q^2 C(\tau/Q^2)$, which agrees well with Equation 12.

From the self consistent solution we can also calculate the distribution of strain *lifetimes*, where the lifetime of a strain i, denoted $\mathcal{T}_i$, is the number of evolutionary epochs for which it has nonzero abundance. In Appendix J we find a distribution

$$p_{\mathcal{T}}(\mathcal{T}) = \frac{2b}{\pi\sqrt{e^{2b\mathcal{T}}-1}}. \qquad (14)$$

Figure 9C observes good agreement between this analytical result and our numerics. $p_{\mathcal{T}}(\mathcal{T})$ decays exponentially at large $\mathcal{T}$ as expected; it additionally has an integrable divergence as $\mathcal{T} \to 0$, due to the distribution of invaders having a constant density at low abundance—these invaders go extinct very quickly as discussed in Section IV B.

The dynamic cavity method also enables us to determine the distribution of strain abundances in steady state, as the solution to a Fokker Planck equation with a vanishing boundary condition at $\nu = 0$ from the absorbing boundary at extinction, and with a source term for the invading strains (Equation J11). In Figure 10 we contrast the scaled distribution of abundances in the Red Queen phase—which agrees well with our analytical solution—with the same distribution for a saturated assembled community with $L = \hat{L}$. There is a marked difference between the two: in the assembled community the abundance distribution is a truncated gaussian while in the Red Queen steady state, the density of strains vanishes at low abundance due to the constant jostling of the ecosystem by invaders which knock low-abundance strains extinct as anticipated in Section IV B.

D. General cavity formulation

We now generalize the cavity analysis away from $\gamma = \Sigma = 0$. For $\gamma \neq 0$ in the LV model (or $\kappa \neq 0$ in the linearized model) the analysis is particularly complicated. The bias and abundance of a focal strain are no longer simply related as in the $\gamma = 0$ case, due to the feedback of the strain on itself via its influence on the other strains. $\nu_0(T)$ will depend both on its bias $\xi_0(T)$ and an additive term arising from the feedback integrated over all times since its invasion. Therefore the analog of Equation 9 for $\gamma \neq 0$ is

$$\nu(T) = \frac{\phi(T)}{Q} \mathbb{1}\left[\phi(T') > 0 \; \forall \; T' \in (\mathbb{T}, T)\right] \tag{15}$$

where

$$\phi(T) = \xi(T) + \gamma \int_{\mathbb{T}}^{T} dT' M(T - T')\nu(T') \tag{16}$$

with $M(\tau)$ a memory kernel that must be determined self-consistently. It will include an instantaneous—on evolutionary time scales—part from the invader's *ecological* feedback on its own abundance, in addition to a slow memory part that extends over many epochs [16]. Both the memory effects and the $s - \Upsilon$ part of ξ mean that the cavity strain will not go extinct when ζ goes through zero, but at some other time when $\phi(T)$ first goes negative.

The statistics of the drives $\zeta(T)$ are determined by the extant community, but $C(\tau)$ is no longer a simple exponential. Nevertheless, one can write an effective stochastic equation for ζ:

$$\frac{d\zeta}{dT} = -\int_{\mathbb{T}}^{T} dT' B(T - T')\zeta(T') + \sqrt{2J}\eta(T) \tag{17}$$

with $B(\tau)$ another memory kernel and $\eta(T)$ still white noise which represents the diffusion-like effects of an invader on the other strains discussed in Section IV B. The Laplace transform of B is related, via a Weiner-Hopf factorization, to the Fourier transform of C.

In principle, to proceed one assumes a $C(\tau)$—or equivalently a $B(\tau)$ and J—as well as an $M(\tau)$ and Υ. Then one computes $\langle \nu(T)\nu(T + \tau)\rangle$ conditioned on invading at time $\mathbb{T}$. By averaging over $\nu(\mathbb{T})$, $\mathbb{T}$ and s, one can enforce the self-consistency of $C(\tau)$ from Equation 10, as for the $\gamma = 0$ case. $M(\tau)$ is then self-consisted from calculating the response of ν to a change in its bias, and Υ is self-consisted to ensure $\sum_i \nu_i = 1$. In the linearized model with resources, the resources have to be handled by a cavity method as well but their effects can be integrated out to give a more complicated relation between the response of strains and M, with γ replaced by κ^2.

Unfortunately, even numerical analysis of the self-consistency conditions to determine the memory functions M and B is likely challenging [44]. However the above structure allows us to glean some insights.

In the absence of selective differences, all strains are statistically similar and the systematic decrease in ζ should make the strain lifetime distribution decay exponentially at long times. This suggests that both the memory kernels M and B will decay exponentially at long times, as will the correlation function of the drives, $C(\tau)$. To explore the effects of feedback, simulations of the $\Sigma = 0$ LV model for $\gamma = -0.8$, 0, and 0.5 were carried out with $C(\tau)$ plotted in Figure 18. We see that $C(\tau)$ indeed decays exponentially at long times for all these γ values, with some deviations, as expected, at shorter times in opposite direction for positive and negative γ. Concomitantly, as γ increases, the timescale over which $C(\tau)$ decays, scaled by the overall turnover time of $\overline{L}$ epochs, grows.

There is no sign of marginality in the exact solution for $\gamma = \Sigma = 0$—therefore the Red Queen phase should be robust to small perturbations, as evinced by these simulations for $\gamma \neq 0$. The heuristic arguments below suggest that the robustness extends to arbitrarily large Σ, and numerical results suggest that it extends also to all $\kappa < 1$ for the linearized model and up to modest—although *not* all—γ in the LV model: see Section V.

E. Effects of selective differences

We have observed in simulations that a Red Queen phase obtains for $\Sigma > 0$ in both the linearized and LV models, with many properties for nonzero Σ similar to the $\Sigma = 0$ case we have analyzed. Here we discuss more systematically the effects of a distribution of general fitnesses, focusing first on the correlation function $C(\tau)$, whose decay at large τ is dominated by strains with anomalously large s. We then consider large Σ and give scaling arguments for how the community evolves into the tail of the s distribution—this allows us to find the dependence of $\overline{\Upsilon}$ and $\overline{p_{inv}}$ on Σ. All of these steady-state properties—including the decay of $C(\tau)$—are determined by the behavior of the $p(s)$ distribution at large s—thus we also consider non-gaussian $p(s)$.

Correlation function for $\Sigma > 0$: From the general structure of the cavity analysis, we can understand the behavior of a strain with anomalously large s. This is simplest for $\gamma = 0$ for which the only memory is in $\zeta(T)$, which still has mean zero. Extinction occurs when $\xi \searrow 0$, i.e. $\zeta \searrow \Upsilon - s$ which is unlikely for large s: for $s - \Upsilon \gg \mathrm{Std}[\zeta]$, ξ will fluctuate around $s - \Upsilon$ staying for a long time far from zero. The rare event for ζ to decrease to $\Upsilon - s$ has, quite generally for a stationary gaussian process, probability of order $\sim e^{-k(s-\Upsilon)^2/\,\mathrm{Var}[\zeta]}$ with the coefficient k depending on the statistics of ζ governed by $B(\tau)$. The correlation function of a strain with general fitness s_i therefore decays exponentially with a timescale that is gaussian-long in s_i. With a distribution of general fitnesses that extends out to large s, the average of $C(\tau)$ over all the strains is dominated at long τ by the fraction of strains whose lifetime is longer than τ. For gaussian $p(s)$ the long-lived strains are gaussian-rare in s and have a lifetime that is gaussian-long in s: averaging over $p(s)$ then yields a $C(\tau)$ that decays as a Σ-dependent power law for large τ, as shown in Appendix K. For an exponential $p(s)$, we find that $C(\tau) \sim e^{-k\sqrt{\log \tau}}$ for Σ-dependent k, which decays slower than any power law.

Associated with the long tail of the correlation functions will be long tails to the memory functions. Thus for γ or κ non-zero and $\Sigma > 0$, it is not obvious that the persistent memory in $M(\tau)$ will not change the behavior qualitatively.

To explore the effects of increasing Σ when $\kappa > 0$, in Figure 18A $C(\tau)$ is plotted for gaussian $p(s)$ for various Σ in the linearized model with $\kappa = 0.8$, and one sees a slower decay of $C(\tau)$ for increasing Σ. Thus we conjecture that the feedback-induced memory effects do not fundamentally change the effects of anomalously large s's in the communities.

Evolutionary transients and steady state for $\Sigma > 0$*:* We now analyze the evolutionary behavior in the limit of large Σ. In what follows we will mainly discuss the linearized model in which the distribution of biases has $\mathcal{O}(\sqrt{D/L}) = \mathcal{O}(1)$ width—our discussion can be generalized by recalling that in the LV model, the width of the bias distribution is $\mathcal{O}(1/Q)$ in the Red Queen phase.

For $\Sigma \gg 1$, there is a long evolutionary transient, with the distribution of extant s_i creeping into the tail of $p(s)$ during this transient period. The tail of $p(s)$ therefore determines the long term evolutionary dynamics, including—when it occurs—the properties of the Red Queen phase. As the population-mean s_i (and therefore Υ) increases, the Υ-dependent scale of the extant s_i distribution is of order

$$\Delta(\Upsilon) \equiv \mathrm{E}[s_a - \Upsilon | s_a > \Upsilon] \approx -\left[\left. \frac{d \log p(s)}{ds} \right|_{s=\Upsilon} \right]^{-1}, \quad (18)$$

which decreases with increasing Υ for $p(s)$ decaying faster than exponentially and increases with Υ for $p(s)$ decaying more slowly than exponentially. At any point in the evolution, if the distribution of extant s_i is concentrated around Υ, the system behaves like there is an exponential distribution of the s_i, with scale $\Delta(\Upsilon)$.

Given this exponential approximation to the general fitness distribution, it will be helpful to understand the behavior of an *assembled* community with an exponential $p(s)$—this will determine a key relationship between L and Υ. If we assemble a large number of strains with an exponential distribution of general fitnesses $p(s) = \frac{1}{\Delta} e^{-s/\Delta}$, for sufficiently large Δ the ecological cavity analysis (see Appendix H) yields an assembled community with $L = \kappa D/\Delta$ in the linearized model (and $L = Q/\Delta$ in the LV model). We therefore expect that during the transient evolution, the community will reach a slowly-changing quasi steady-state with diversity given, at any point in time, by $\kappa D/\Delta(\Upsilon)$.

Therefore the behavior of Υ determines the behavior L. How does Υ depend on T during this transient and steady state of the evolution? The increase of Υ is tied to the increasing population-mean s, denoted $\langle s \rangle \equiv \sum_i \nu_i s_i$, so we are led to analyze how $\langle s \rangle$ changes in evolutionary time. Each successful invader a must have $\zeta_a + s_a > \Upsilon$. The probability density of s_a conditioned on invasion is

$$p(s_a | \text{invasion}) \approx \frac{1}{\Delta} \exp\left[-\frac{s_a - \Upsilon}{\Delta} - \frac{\sigma_a^2}{2\Delta^2} \right] \Phi\left[\frac{s_a - \Upsilon}{\sigma_a} \right], \quad (19)$$

where $\sigma_a^2 \equiv \mathrm{Var}[\zeta_a] \approx D/L$ and Φ is the CDF of the standard normal distribution. It follows that

$$\mathrm{E}[s_a - \Upsilon | \text{invasion}] = \Delta(\Upsilon) - \frac{\sigma_a^2}{\Delta(\Upsilon)}. \quad (20)$$

As a result, when $\Delta(\Upsilon) \approx \sigma_a \approx 1/\kappa$, there is a steady state and Υ is roughly constant in evolutionary time, with its value depending on the form of the function $\Delta(\Upsilon)$. Meanwhile, $\overline{L} \sim \kappa D/\Delta(\Upsilon) \sim \kappa^2 D$.

We can now proceed to analyze the behavior of a family of distributions $p(s) \sim e^{-(s/\Sigma)^\psi/\psi}$, for which $\Delta(\Upsilon) \approx \Sigma^\psi/\Upsilon^{\psi-1}$. For stretched exponential decay of $p(s)$, corresponding to $\psi < 1$, $\Delta(\Upsilon)$ is an increasing function—therefore Υ will run away to positive values with L concomitantly decreasing. The diversity crashes and eventually the community will reduce to a single strain that goes extinct when a fitter strain invades.

For $\psi > 1$ (including the gaussian case $\psi = 2$), initially Δ is of order $\Sigma \gg 1$. From the above analysis, we expect diversity $L \sim \kappa D/\Delta$. With Δ large, invasions will tend to increase Υ, thereby decreasing Δ and increasing L. Eventually Δ will decrease to $\overline{\Delta} \sim \sqrt{D/L} \sim 1/\kappa$, independent of ψ, so that the widths of the extant s_i and ζ_i distributions are comparable. Concomitantly, L will saturate at $\overline{L} \sim \kappa D/\overline{\Delta}$, and Υ will saturate at $\overline{\Upsilon} \sim (\Sigma^\psi/\overline{\Delta})^{1/(\psi-1)}$, with $\log \overline{p_{inv}} \sim (\Sigma/\overline{\Delta})^{\psi/(\psi-1)}$.

We are now in a position to analyze the transient evolutionary dynamics that occur for large Σ and $\psi > 1$. For large Δ, the change in Υ due to a successful invasion by strain a is roughly $\Delta(\Upsilon)/L$, coming from the fitness increment multiplied by the $\mathcal{O}(1/L)$ typical abundance ν_a. Since the fitness increment is $\sim \Delta$ and $1/L \sim \Delta/D$, the change in Υ per invasion is $d\Upsilon/dT \sim \Delta(\Upsilon)^2/D$. On average $d\Upsilon/dT$ is positive until the contribution of ζ_a becomes comparable to $s_a - \Upsilon$, at which point $\Upsilon = \overline{\Upsilon}$ and $\Delta = \overline{\Delta}$.

The transient behavior is found by integrating up the typical change per invasion: roughly $d\Upsilon/dT \sim \Delta(\Upsilon)^2/D \sim \Sigma^{2\psi}/D\Upsilon^{2\psi-2}$ until Υ is close to $\overline{\Upsilon}$. Thus during the transient

$$\Upsilon \sim \left(\frac{\Sigma^{2\psi} T}{D} \right)^{\frac{1}{2\psi-1}} \quad (21)$$

$$\frac{L}{D} \sim \Sigma^{-\frac{\psi}{2\psi-1}} \left(\frac{T}{D} \right)^{\frac{\psi-1}{2\psi-1}} \quad (22)$$

for a time

$$T_{transient} \sim D\Sigma^{\psi/(\psi-1)}, \quad (23)$$

after which the steady state ensues.

An important observation is that some aspects of the Red Queen steady state for large Σ are *independent of details* of the s distribution and of Σ: in particular, for large Σ, $\overline{L}$ is independent of Σ, as seen in Figure 4 for gaussian $p(s)$, since $\overline{\Upsilon}$ becomes large enough that the distribution of the extant s_i has $\mathcal{O}(1)$ width, irrespective of Σ.

To compare with our numerics for gaussian $p(s)$, we specialize to $\psi = 2$ in which case $\Delta(\Upsilon) \approx \Sigma^2/\Upsilon$. Here we have $\overline{\Upsilon} \sim \Sigma^2$ and $\overline{p_{inv}} \sim e^{-q\Sigma^2/2}$ for q having some κ-dependence. This scaling is similar to the saturated assembled community (Section IV A), in which $-\log \hat{S} \sim \Sigma^2$ was conjectured to scale with $\log \overline{p_{inv}}$. During the long initial transient, $\Upsilon \sim T^{1/3}$ and $L \sim T^{1/3}$ with the transient lasting for a number of epochs $T_{transient} \sim D\Sigma^2$, consistent with the rapid growth of transient length with Σ in Figures 4, 5 and 6.

Because of large κ-dependent coefficients, even moderate values of Σ can produce unrealistically small values of $\overline{p_{inv}}$.

For $\Sigma = 1$, $\rho = 0$ and $\kappa = 0.8$, the invasion probability at steady state is less than 10^{-15} (Figure 5D) which suggests that $\overline{\Delta}$, which determines $\overline{\Upsilon}$ via $\overline{\Upsilon} \sim \Sigma^2/\overline{\Delta}$, has a value $\overline{\Delta} \cong 0.12$ for $\kappa = 0.8$, substantially smaller than the value for the top-down assembled community, $\overline{\Delta} = (1-\kappa^2)/\kappa = 0.45$ (Equation 8a).

In the CR model, invasion probabilities are even smaller: as discussed earlier, the width of the general fitness terms dominates over that of the interactions by a factor of $\sqrt{D}$, corresponding to $\Sigma \sim \sqrt{D}$ in the linearized model. Therefore $\overline{p_{inv}}$ is exponentially small in D. Indeed we see (Figure 2B) that for $\kappa = 0.4$ and $D = 50$ in the CR model, the invasion probability in steady state is $\sim 10^{-400}$, where here the distribution of general fitnesses U_i inherits its gaussian distribution from the ensemble of the $\mathcal{G}$ matrix that we considered.

Generally distributions with faster-decaying tails but similar Σ have higher invasion probability at steady state. However even in the limit $\psi \to \infty$ which corresponds to a double exponential decay $p(s) \sim \exp(-\exp(s/\Sigma))$, $\overline{p_{inv}}$ still decays exponentially in Σ and therefore as a stretched exponential in D, for the CR model.

For distributions that have a sharp cutoff at some maximum s, the invasion probability in steady state is not so small, even with a broad distribution of s's. If $p(s) \sim (\Sigma - s)^\lambda \Theta(s)\Theta(\Sigma - s)$ for large Σ and some power λ then the width of the extant s_i distribution scales as $\frac{1}{\lambda+2}(\Sigma - \Upsilon)$. The Red Queen phase obtains when the distribution of extant s has $\mathcal{O}(1)$ width, in which case $\overline{p_{inv}} \sim 1/\Sigma^{\lambda+1}$, which gets small much more slowly with Σ than the exponential—or steeper—dependence for the family $p(s)$ tuned by ψ, described above. Importantly, once the Red Queen steady state is established, the population-mean s, denoted $\langle s \rangle$, does not creep ever closer to the cutoff at the maximum s. This is in important contrast to the situation with $\kappa = 1$, where Υ would inch up as $\langle s \rangle$ increases towards the maximum s, since the Lyapunov function Υ has a part that is exactly $\langle s \rangle$.

We have found that there is a wide range of scalings of $\overline{\Upsilon}$ and $\overline{p_{inv}}$ with Σ in the linearized model or with D in the CR model, that can be reasonably obtained with different distributions of the s_i or the elements of $\mathcal{G}$ and $\mathcal{F}$. We have used gaussian distributions since they allow us to easily draw invaders conditioned on having positive invasion fitness, and to explore issues of *principle* regarding the Red Queen phase. However it is important to note that quantitative aspects such as the scaling of the invasion probability with D are very non-universal.

V. DISCUSSION

In this work we have explored evolution in a range of ecological models which exhibit diverse stable communities, and found that generically, after a transient period of evolution, the community converges to a Red Queen state of constant turnover with the probability of new strains successfully invading constant. In contrast to previous work which finds such behavior in host-pathogen interactions [25, 45, 46], here the interactions are competitive—mediated by resources—rather than predator-prey-like. There is not a clear notion of kill-the-winner dynamics in which one subpopulation "chases" the other through trait space; nonetheless constant turnover ensues. The evolving ecology acts as a concrete manifestation of the environmental feedback that engenders continual Red Queen evolution in random landscape models [16] without diversity. The consumer resource model and a linearized approximation to it display a Red Queen phase as long as the consumption and growth are not perfectly correlated ($\kappa < 1$) and the Lotka Volterra model also has a Red Queen phase but only for symmetry parameter less than a critical value.

Importantly, the Red Queen phase persists in the presence of arbitrarily large general fitness differences s_i provided that their distribution falls off faster than exponentially for large s. Previous analyses of high-dimensional ecological models [18, 32] have, as noted earlier, assumed that in the large D (or similar) limit, the distribution of general fitnesses (or similar quantities) decreases as $1/\sqrt{D}$ and taken the then-well-behaved large D limit. We have shown that this assumption is not needed: In a long-evolved community, the width of the distribution of general fitness differences *within the evolved community* will become comparable to the variations among the strains of the effects of the ecological interactions. Even starting with a parametrically (in D) broad distribution of general fitnesses, some properties of evolved communities are independent of the distribution, though other properties (such as the invasion probability of new strains) are affected.

If the distribution of the s_i falls off with a large characteristic scale—which occurs naturally in the CR model—there is a long transient period during which evolution is initially dominated by increases in s and the diversity is gradually increasing as the population moves out into the tail of the s distribution. The transient behavior finds a steady state when the strain-to-strain variations of s_i and the ecological influences of other strains in the community are comparable—here the diversity of the Red Queen steady state becomes independent of the distribution of s, but the invasion probability at steady state can be extremely small. However if there is a maximum to s, perhaps with a rapidly decaying distribution extending beyond this, the invasion probability, and hence the community turnover rate, stabilizes at a value that need not be small.

Below, we discuss some unresolved issues from the current work and suggest future directions.

Other well-mixed eco-evolutionary phases: What other long term states occur naturally and robustly in eco-evolutionary models without any spatial structure or externally varying environment? For models with perfect symmetry, such as the $\kappa = 1$ CR and linearized models, the presence of a Lyapunov function means that the community can continue to evolve and turnover but will get slower and slower. Does this also occur away from such special points? In the simple CR models with a convex Lyapunov function, the Red Queen phase appears to replace such a state as soon as $\kappa < 1$. However for LV models, we have found evidence for a gradually slowing phase for a range of $\gamma > \gamma_c$. However this phase which we have dubbed an *oligarch* phase has surprising features that we do not understand.

As first mentioned in Section III E, the eco-evolutionary

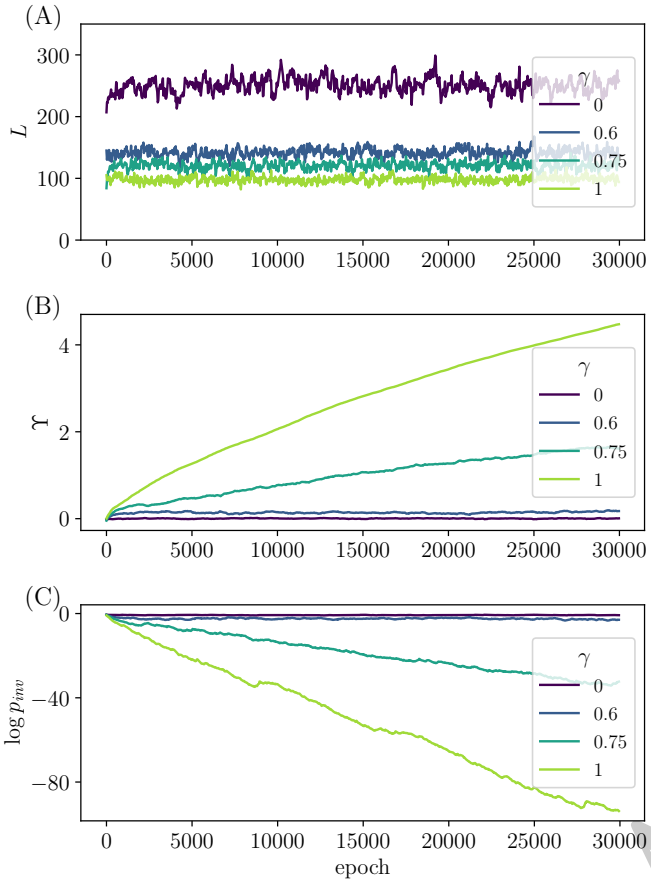

Figure 11. The mode of evolution in the LV model undergoes a transition around $\gamma_c \approx 0.65$, with the crossover observed to sharpen for increasing Q (not shown). Here we show behavior of L, Υ and p_{inv} in both eco-evolutionary phases of the LV model. (A) L is roughly constant in both the Red Queen and the oligarch phase. (B) Υ fluctuates around a steady state in the Red Queen phase for $\gamma < \gamma_c$ and increases without bound in the oligarch phase for $\gamma > \gamma_c$. (C) Concomitantly, p_{inv} achieves a steady state in the Red Queen phase and is ever-decreasing in the oligarch phase. $Q = 20$ and $\Sigma = 0$ throughout.

dynamics of the LV model undergo a sharp qualitative change as a function of γ, around $\gamma_c \approx 0.65$ for $\Sigma = 0$. We have not investigated the dependence of γ_c on the width Σ of the general fitness distribution, but have checked that there are still two distinct phases for $\Sigma > 0$: thus the transition appears robust.

For $\gamma < \gamma_c$, the Red Queen phase obtains and there is continuous turnover with the mean general fitness, Υ, and the invasion probability, p_{inv}, roughly constant. By contrast, for $\gamma > \gamma_c$, we find a phase in which Υ is an ever-increasing function of the number of invasions, and there is no steady state, with the community becoming progressively harder to invade. This transition is not apparent in the dynamics of the diversity L, which is still roughly steady over time, but shows up in the dynamics of Υ and p_{inv} (Figure 11).

Most strikingly, the abundance trajectories of the strains on evolutionary timescales becomes very different with a few strains—the oligarchs—becoming far more abundant than the others. Figure 12 shows the abundance dynamics

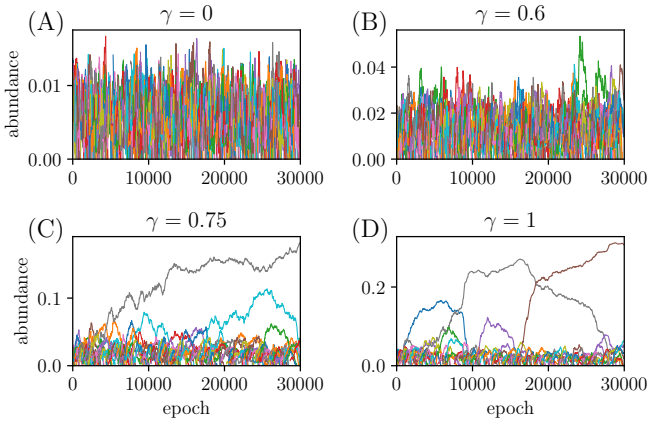

Figure 12. Strain trajectories in the LV model, in both the Red Queen and oligarch phases. (A)–(D) show the behavior of selected strain trajectories for two values of γ below the transition and two values above the transition. In the small-γ regime we find a Red Queen phase, while in the large-γ regime—which we call the "oligarch phase"—there are strains into which an $\mathcal{O}(1)$ fraction of the total abundance condenses, though these strains continue to turn over more and more slowly. $Q = 20$ and $\Sigma = 0$ throughout.

in both the Red Queen and oligarch phases, and Figure 11 shows the corresponding trajectories of L, Υ and p_{inv}. For $\gamma = 0$ and 0.6, the constant turnover of the Red Queen phase is manifest in the narrow distribution of lifetimes for the strains in the community, while for $\gamma = 0.75$ and 1, the dynamics look qualitatively different with a few strain abundances running away to large values, though these oligarch strains still slowly turn over. In the oligarch phase, an $\mathcal{O}(1)$ fraction of abundance condenses into an $\mathcal{O}(1)$ number of strains and Υ continues to increase with p_{inv} concomitantly decreasing.

Qualitatively, the oligarch phase appears to occur due to feedback between the abundant strains and the invaders: if a prospective invader a is to successfully enter the community it must have a positive contribution to its invasion fitness from an abundant strain, say, ℓ i.e. $V_{a\ell} > 0$. Then since γ is strongly positive, it will tend to have $V_{\ell a} > 0$ as well, thus the invader strain will increase the abundance of the oligarch strain ℓ, but this does not explain the turnover of oligarchs. The non-steady-state nature of the oligarch phase makes analysis difficult since correlation and response functions of strain abundances in evolutionary time must involve two times. However we do find a related steady state behavior for $\gamma < \gamma_c$ that might give clues.

The transition between the Red Queen and oligarch phases appears to be first order-like, with hysteresis observed if one changes γ across γ_c (Figure 16). Strikingly, if one evolves with $\gamma > \gamma_c$ for some time, and then rapidly quenches to $\gamma < \gamma_c$, one can obtain a steady state which exhibits aspects of both the Red Queen and oligarch phases. A handful of high-abundance strains persist at roughly constant abundance without turning over, while the majority of strains turn over steadily as they would in the"normal" Red Queen phase. In this coexisting state between the two phases, Υ remains elevated and p_{inv} remains suppressed

relative to their values in the Red Queen phase, while L is roughly constant (Figure 16). Further analysis of such a steady oligarch state could lead to a better understanding of the oligarch phase as well as the transition between the two eco-evolutionary phases.

What classes of models can exhibit an oligarch phase? Naively, the heuristic argument above would suggest an oligarch phase in the linearized model, though such a phase does not seem to exist. This difference in behaviors may be related to the phase diagrams of the *totally symmetric* LV and linearized models: the linearized model always has a convex Lyapunov function whereas the LV Lyapunov function becomes non-convex for sufficiently large S [42]. What other phenotype models—with interaction via chemicals—can display an oligarch phase of eco-evolutionary dynamics?

Parent-mutant correlations: In this work, we have primarily studied a process that is not strictly speaking evolution: new strains that are introduced are unrelated to extant strains. The crucial feature that makes our model different from well-studied models of top-down assembly is that strains extinctions are permanent, which qualitatively changes the shape of the abundance distribution: few strains with low abundance exist as these are most easily driven extinct by invasion-induced perturbations.

We have shown that introducing mutant strains related to extant parental strains results in very similar behavior if the mutant and parent are not strongly correlated phenotypically.

However if the effects of mutations are small—surely relevant biologically [47]—diversification is slower because of the increased importance of general fitness differences. How do the existence and properties of a diverse Red Queen phase depend on the magnitude of the mutational effects as correlation between mutant and parent phenotypes approaches unity? What kinds of dynamics obtain for a distribution of mutational effect sizes? What is the interplay between general fitnesses and parent-mutant correlations? What are the phylogenies generated by the Red Queen eco-evolutionary process? Do they resemble any known class of coalescent trees? These issues will be addressed in a future paper.

Changing environments The CR and linearized models naturally allow study of how evolving communities are affected by extrinsic changes in the environment. During the initial transient period of evolution before the Red Queen phase obtains, the community in the CR model adapts to its resource supply by aligning the growth vectors of strains (rows of $\mathcal{G}$) with the resource supply vector $\mathbf{K}$. If the supply vector $\mathbf{K}$ changes extrinsically after this initial period of evolution, the distribution of U_i will broaden and the diversity will crash, only to rebuild as the community readapts to the new resource supply vector. This scenario can be studied in the linearized model if we parameterize the general fitnesses through an interaction with the environment, and define the resource vector as $R_\alpha = K_\alpha - \sum_j F_{j\alpha}\nu_j$, for resource supply $\mathbf{K}$. This parameterization gives rise to selective differences $s_i = \sum_\alpha G_{i\alpha}K_\alpha$. Therefore changing $\mathbf{K}$ will affect the s_i. What do the eco-evolutionary dynamics look like for a continually changing supply vector, either driven extrinsically or through some further feedback from the ecological community? Can this externally driven continual evolution be distinguished from the self-driven Red Queen phase?

Clonal interference: In this work we have taken advantage of a separation of timescales between evolution and ecology. However such a separation is not at all guaranteed to exist, particularly in host-pathogen systems [48], or in large populations with abundant supply of mutations [8], or when mutational effects are small enough that ecological timescales are slow. Investigation of the dynamics of ecological models in a "clonal interference" regime, with multiple ecological mutants emerging before any single one of them has reached its fixed point abundance, is an open challenge of definite relevance to biological systems.

Spatial structure: Spatial structure with spatial transport remains an understudied—although crucial—feature of ecological and evolutionary models. Gut and skin microbiota associated with different individuals are realizations of distinct ecological communities coupled by migration, with new mutants arising locally with the potential to spread across people [49, 50].

We have found that even without spatial structure, the behavior is quite rich. However generalizing our analyses to spatial-mean-field-like "island" models with all-to-all migration—roughly like microbes from person-to-person—or to finite dimensional spatial structure and dynamics is a very interesting direction. Can a diverse Red Queen phase exist if there is only migration of strains between identical spatial patches, but no evolution? Or is evolution required to keep generating new types and produce turnover of biodiversity? If the niche parameter (D or Q^2 in our model) is not large enough for all the strains in the system to coexist locally, then different strains could still inhabit different spatial locations. Is this heterogeneity maintained when strains migrate between spatial patches, and when evolution continually produces new variants? How high persistent diversity can be maintained? In particular how doe this grow with the spatial size or with the number of microbiome hosts?

Other spatiotemporal eco-evolutionary phases: The range of models we have studied in this work hints at the generality of the Red Queen phase in ecological models with stable communities. However, ecologically chaotic dynamics constitute another ecological phase for which understanding its evolution is also a compelling goal. In previous work [37] we have studied gradual evolution and assembly in a spatiotemporally chaotic community, where the spatial structure stabilizes the fluctuating ecological dynamics from extinctions. In the simplest predator-prey like models that yield this phase, there are no niches in the sense of those created by different resources: the model corresponds to a $Q = 0$ Lotka Volterra model. However the dynamical nature of the ecological phase allows one to pack unlimited diversity into a single "niche," even when strains are added gradually through evolution. With the presence of general fitness, one can still diversify to arbitrarily large L, but evolution slows down, with p_{inv} becoming arbitrarily small and Υ arbitrarily large.

We can understand the tendency towards unlimited diversity from the phase diagram of the top-down assembled community. If one starts in the unstable phase, then in-

creasing the diversity does not bring one closer to the phase boundary between stable and unstable phases; in fact it takes one further from this boundary. Therefore there is no divergent fragility that limits the community's diversity. By contrast, for the stable dynamics studied here, the presence of niches sets a scale for the diversity which is $\overline{L} \sim D$ in the CR and linearized models, and $\overline{L} \sim Q^2$ in the LV model. These niches qualitatively change the outcome of the evolutionary dynamics: the nature of the ecology is seen to have a drastic effect on community evolution and diversification.

Diversity across scales: Experimental data have shown that strain dynamics can differ based on the resolution at which they are observed, with closely related strains undergoing larger fluctuations than family-level groupings [47, 51]. Further study of ecological dynamics across scales of diversity is needed. How—hopefully already in simple models—does evolution create diversity over many scales, and how does this diversity interact with the ecological dynamics across such scales? Can evolution robustly lead to ecologically chaotic dynamics of the micro-diversity but stable dynamics at coarser levels of differentiation?

Prospects: The models and scenarios described in this work provide a simple framework and examples in which ecological interactions produce an eco-evolutionary Red Queen phase. The analytical tractability of the models in the simplest case—and the generality and robustness of the Red Queen phase we have found—indicates that the study of simple models might advance our understanding of the evolution of fine-scale biodiversity in natural microbial communities.

ACKNOWLEDGMENTS

We thank Gabriel Birzu for illuminating discussions. This research was supported in part by the National Science Foundation (NSF) via NSF PHY-2210386 to DSF. AM and DSF acknowledge support from the Kavli Institute for Theoretical Physics (KITP) through the Gordon and Betty Moore Foundation Grant No. 2919.02, NSF PHY-1748958 and PHY-2309135, the Heising-Simons Foundation, and the Simons Foundation (216179, LB). We thank the Stanford Sherlock cluster for computing resources.

Appendix A: CR model

The Lyapunov function of the CR model when $\mathcal{G} = \mathcal{F}$ is

$$\Lambda = -\sum_\alpha \left[K_\alpha \log \frac{K_\alpha}{\mathcal{R}_\alpha} - (K_\alpha - \mathcal{R}_\alpha) \right] \tag{A1a}$$

$$\text{with } \mathcal{R}_\alpha = \frac{K_\alpha}{\omega + \sum_{j=1}^S \mathcal{F}_{j\alpha} n_j}. \tag{A1b}$$

Λ is increasing along the dynamics of Equation 1 [33].

In order to study the CR model in more detail, it is useful to identify the combinations of parameters that matter for its fixed point. We make the choice $\omega = 0$, which does not qualitatively change the behavior, but simplifies the model. Then we define $\tilde{\mathcal{R}}_\alpha = \mathcal{R}_\alpha \mu_g / d$, $\tilde{\sigma}_g = \sigma_g/\mu_g$, $\tilde{\mathcal{G}} = \mathcal{G}/\mu_g$, $\tilde{\sigma}_f = \sigma_f/\mu_f$, $\tilde{\mathcal{F}} = \mathcal{F}/\mu_f$ and $\tilde{K}_\alpha = \mu_g K_\alpha / d\mu_f$, such that Equation 1 becomes

$$\frac{dn_i}{d(mt)} = n_i \left(\sum_\beta \tilde{\mathcal{G}}_{i\beta} \tilde{\mathcal{R}}_\beta - 1 \right) \tag{A2a}$$

$$\frac{d\tilde{\mathcal{R}}_\alpha}{d(\mu_f t)} = \tilde{K}_\alpha - \tilde{\mathcal{R}}_\alpha \sum_j \tilde{\mathcal{F}}_{j\alpha} n_j. \tag{A2b}$$

Therefore κ, $\tilde{\sigma}_g$, $\tilde{\sigma}_f$ and the rescaled supply vector $\tilde{\mathbf{K}}$ are the only quantities that matter for the fixed point abundances. We can set $\mu_f = \mu_g = 1$ and $d = 1$ without loss of generality. The fixed point abundances $\{n_j^*\}$ and $\{\mathcal{R}_\alpha^*\}$ satisfy the equations

$$\sum_\beta \mathcal{G}_{i\beta} \mathcal{R}_\beta^* = 1 \;\; \forall i \in \mathcal{C}; \quad \mathcal{R}_\alpha^* = \frac{K_\alpha}{\sum_j \mathcal{F}_{j\alpha} n_j^*}. \tag{A3}$$

We do not expect that the variance of the components of $\mathbf{K}$ plays an important role, so we set $K_\alpha = K$. The value of K matters only insofar as it determines the scale of the $\{n_j^*\}$, which can be rescaled to eliminate K. Therefore in our simulations we set $K = 1$.

Appendix B: Parent-mutant correlations in CR model

We can draw mutant phenotypes to be correlated with the phenotype of a parent, which is chosen with probability proportional to its abundance for each epoch. Given the parent phenotype—the vectors $\mathcal{G}_P$ and $\mathcal{F}_P$—we draw a mutant phenotype $\mathcal{G}_M$ and $\mathcal{F}_M$ which has elementwise Pearson correlation ρ with the parent phenotype. We also enforce correlation elementwise correlation κ between $\mathcal{G}_M$ and $\mathcal{F}_M$. In Figure 13 we show numerical results from this process. The trends are similar to what we observe when we vary ρ in the linearized model and, importantly, show that we still find a Red Queen steady state across a range of ρ, with the phase that obtains looking qualitatively similar to the $\rho = 0$ Red Queen phase. Of particular phenomenological interest is the dependence of $\overline{p_{inv}}$ on ρ, which displays a nonmonotonicity with the initial increase similar to the one observed in the linearized model (Figure 6D). We deliberately stay away from the limit $\rho \to 1$, which is left for future work as additional subtleties arise.

Appendix C: Relation between CR and linearized models

We here connect the CR model to the linearized model, which we have argued captures the behavior of the CR model and is easier to analyze. The linearization of the dependence of $\mathcal{R}^*$ on the $\{n_j^*\}$ is justified when the mean of $\sum_j \mathcal{F}_{j\alpha} n_j^*$ over α is larger than its variations between α. In Figure 14A we show that this condition is met in the evolved community for $\kappa = 0.4$. Figure 14B shows that the total consumer population is roughly constant in evolutionary time, which motivates a description in terms

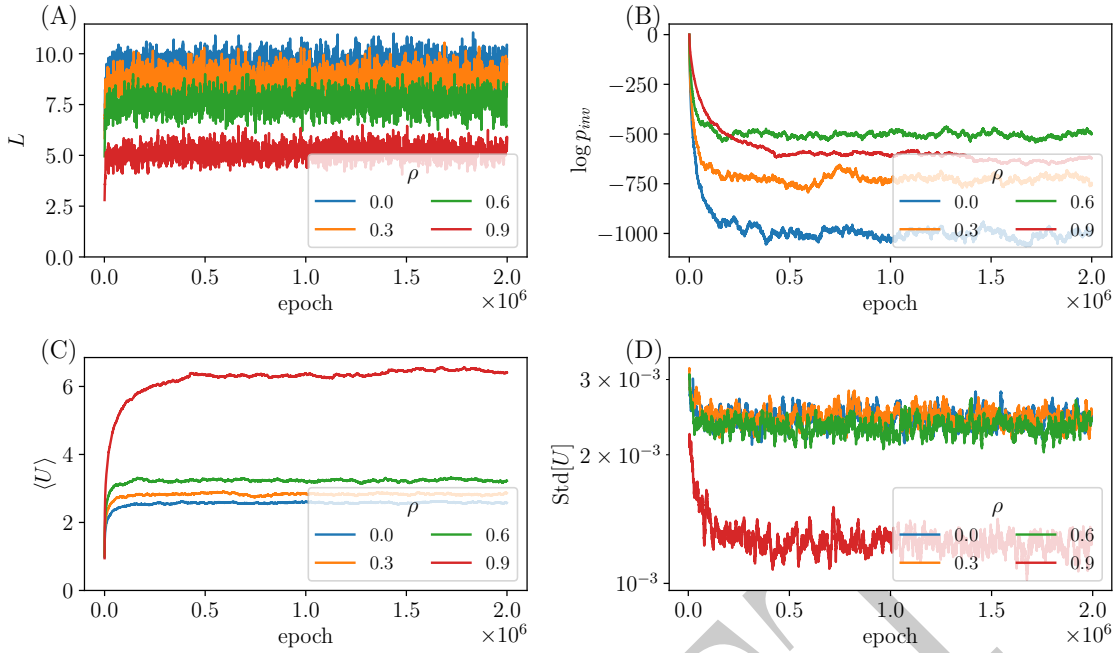

Figure 13. The effect of parent-mutant correlations on evolution in the CR model. (A) $\overline{L}$ is a decreasing function of ρ. (B) $\overline{p_{inv}}$ is a nonmonotonic function of ρ, at first increasing with ρ and then beginning to decrease as $\rho \to 1$. (C) $\overline{\langle U \rangle}$ increases with ρ as the distribution of extant U_i pushes farther into the tail. (D) $\overline{\text{Std}[U]}$ decreases with ρ, as $\overline{L}$ decreases and the distribution of extant U_i becomes narrower.

of fractional abundances for the linearized model. We carry out an expansion which allows us to separate out general fitness and interaction pieces in each strain's growth rate.

In the Red Queen steady state the means of $\mathcal{F}$ and $\mathcal{G}$ are greater than 1 due to evolutionary conditioning—for example in Figure 3A, the plot for $\kappa = 0.4$ shows that the mean of $\mathcal{G}$ plateaus at $\langle U \rangle \approx 2.5$. The mean of $\mathcal{F}$ is smaller than that of $\mathcal{G}$ but still larger than 1. Let us split $\mathcal{F}$ into a mean part and a part with zero mean, such that $\sum_j \mathcal{F}_{j\alpha} n_j = Y + \sum_j f_{j\alpha} n_j$ where the f matrix has zero mean and $Y = \langle \mathcal{F} \rangle N$, with $N = \sum_j n_j$. Angle brackets denote an average over the extant community. Then we can Taylor expand the resource abundances, yielding

$$\mathcal{R}^*_\alpha \approx \frac{K_\alpha}{Y}\left(1 - \frac{\sum_j f_{j\alpha} n_j}{Y}\right). \tag{C1}$$

Therefore at the fixed point the condition on the extant strains that their growth rates vanish becomes

$$0 = \sum_\beta \mathcal{G}_{i\beta} \frac{K_\beta}{Y}\left(1 - \frac{\sum_j f_{j\beta} n_j}{Y}\right) - 1 \text{ for } i \in \mathcal{C} \tag{C2a}$$

$$\implies 0 = \frac{1}{Y}\sum_\beta g_{i\beta} K_\beta - \frac{1}{Y^2}\sum_{\beta,j} g_{i\beta} K_\beta f_{j\beta} n_j - \frac{\langle \mathcal{G} \rangle}{Y^2}\sum_{\beta,j} K_\beta f_{j\beta} n_j + \frac{\langle \mathcal{G} \rangle}{Y}\sum_\beta K_\beta - 1 \text{ for } i \in \mathcal{C}, \tag{C2b}$$

where we have decomposed the $\mathcal{G}$ matrix as $\mathcal{G}_{i\beta} = \langle \mathcal{G} \rangle + g_{i\beta}$ with $g_{i\beta}$ having zero mean. This form allows us to separate out the general fitness and interaction pieces in the growth rate of each strain. On the right hand side of Equation C2b, the first term contains the general fitnesses and is proportional to $U_i - \langle U \rangle$. The second term is the contribution to the growth rate of strain i from the ecological interactions, and the last three terms are i-independent and constitute an effective Lagrange multiplier that keeps N roughly constant when $\langle \mathcal{G} \rangle > \mathcal{O}(1)$.

In the assembled community, $Y = \mathcal{O}(L)$ and the $f_{j\alpha}$ and $g_{i\beta}$ have width σ_f and σ_g respectively. Therefore the width of the general fitness term scales as $\sigma_g\sqrt{D}/L$ and the width of the interaction piece scales as $\sigma_f\sigma_g\sqrt{LD}/L^2$. Since $L = \mathcal{O}(D)$ for sufficiently large S, with each of the n^*_j being $\mathcal{O}(1)$, the distribution of general fitnesses in the assembled community with large S is a factor of $\sqrt{D}/\sigma_f$ wider than than the distribution of drives. Since σ_f and σ_g are $\lesssim 1$ in order to make the majority of entries in $\mathcal{F}$ and $\mathcal{G}$ positive, the general fitnesses dominate in the assembled community. When the community evolves, the $\mathcal{G}_i$ vectors elongate in the direction of the supply vector

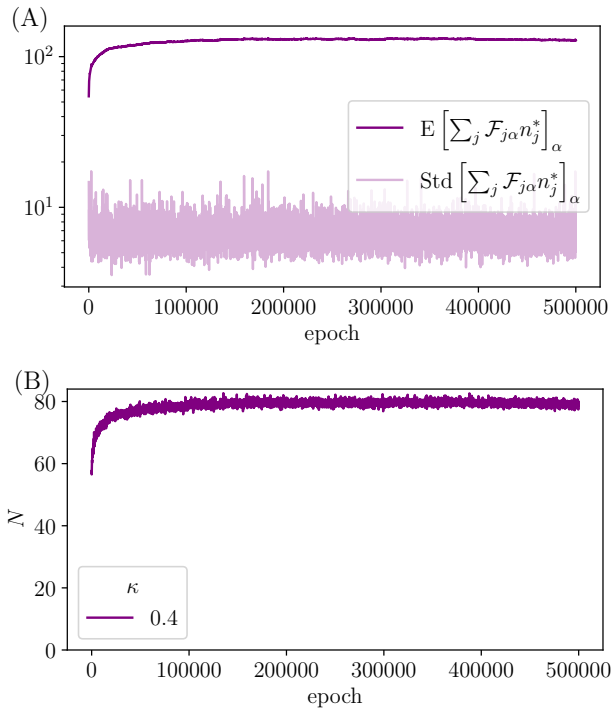

Figure 14. In the CR model, linearization of the resource abundance as a function of consumer abundance is justified, and the total ecosystem population is roughly constant in the Red Queen phase (A) At the steady state, the width (over α) of $\sum_j \mathcal{F}_{j\alpha} n_j^*$ is much smaller than the mean, implying that there is a self-consistent expansion of the variations in this quantity out of the denominator. (B) The total consumer population at the fixed point, $N = \sum_j n_j^*$, is roughly constant over evolutionary time in the Red Queen phase, motivating our parameterization in terms of fractional abundances ν_i. Data are shown for $\kappa = 0.4$; other parameters are the same as in Figure 1.

K, which decreases the width of the distribution of extant $\sum_\beta g_{i\beta} K_\beta / Y$, which is governed by the variations of the $\mathbf{g}_i$ vectors in the direction parallel to K. However the width of the extant drive distribution does not decrease—this allows the distributions of general fitnesses and drives to attain comparable widths when evolved (Section II B).

Appendix D: Algorithm to find fixed point

Integrating the ecological dynamics to find their stable fixed point is too slow to observe many of the features of the evolution that we discuss. In order to probe longer evolutionary trajectories, we have used a heuristic method to find the fixed point; we then check that it is stable and cannot be invaded by any of the extinct strains. Below we describe the algorithm for the linearized and LV models, assuming we are given some interaction matrix V, which can be made to include selective differences by adding s_i to the ith row of V (since $\sum_i \nu_i = 1$). We also comment below on a slight modification of the algorithm for the CR model. The main challenge is to find the set $\mathcal{C}$ of strains in the community that has nonzero abundance at the stable uninvadable fixed point. We accomplish this task with an iterative method that converges most of the time.

1. Initialize $\mathcal{C}$ as the set of all strains in the community (including the new invader if applicable) and initialize the extinct set $\mathcal{E}$ as an empty set. V^* is the submatrix of interactions for the extant strains, and therefore contains the rows and columns corresponding to strains in $\mathcal{C}$.
2. Invert V^* to find a fixed point of the dynamics via $\nu_i^* = \Upsilon^* \sum_j {V^*}^{-1}_{ij}$ and $\sum_i \nu_i^* = 1$ which fixes Υ^*. In general some of the ν_i^* will be negative. Remove the set $\{i | \nu_i^* < 0\}$ from $\mathcal{C}$ and add it to $\mathcal{E}$.
3. Calculate the invasion fitnesses ξ_j of each putatively extinct strain, via $\xi_j = \sum_{k\in\mathcal{C}} V_{jk}\nu_k^* - \Upsilon^*$. Transfer the set of strains $\{j | \xi_j > 0\}$ from $\mathcal{E}$ to $\mathcal{C}$.
4. Iterate steps 2 and 3 until we converge to sets $\mathcal{C}$ and $\mathcal{E}$ such that $\nu_i^* > 0$ for all $i \in \mathcal{C}$ and $\xi_j < 0$ for all $j \in \mathcal{E}$.

One can check stability of the final fixed point by computing the Jacobian of the dynamical equation. The vast majority of the time, the fixed point found in this way is stable.

When the algorithm does not converge within 10 iterations, we stop adding extinct strains with positive invasion fitnesses back into the community, and thereby converge to a fixed point with positive abundances, which is *invadable* by some of the strains that were declared extinct. This adjustment is most often deployed when $\mathcal{E}$ and $\mathcal{C}$ have similar sizes at the fixed point, which can happen for an initial assembled community with large S, or for the evolved state with small κ where $\overline{L}$ is small and each invader can cause $\mathcal{O}(\overline{L})$ extinctions. In these cases the iterative algorithm does not converge reliably. However for small perturbations to the community (as in the case of single invaders with large $\overline{L}$), $\mathcal{E}$ is much smaller than $\mathcal{C}$ and the algorithm converges rapidly. Results from the error-prone regimes regimes of evolution do not play a large part in any of our conclusions.

In the CR model, one cannot simply invert a matrix to find the fixed point for a subset of strains due to the nonlinearity in the interaction. Therefore we use a numerical solver to find the fixed point for a given $\mathcal{C}$—the rest of the algorithm is the same as in the linearized and LV cases.

Appendix E: LV evolution for a range of γ

As in the linearized model, the LV model (shown in Figure 15 for $\Sigma = 0$) exhibits a Red Queen steady state in which $\overline{L}$ is less than its maximal value in an assembled community, $\hat{L} = Q^2/(1+\gamma)^2$, (independent of Σ), as reviewed in Appendix G. The gap between $\hat{L}$ and $\overline{L}$ diverges as $\gamma \to -1$, reflecting the fact that the fragility Ξ is numerically larger for $\gamma \to -1$, and so it drives an average of one strain extinct per invasion for L farther from the point of diverging fragility. We also see that for $\Sigma = 0$ (as in these simulations) $\overline{\Upsilon}$ changes sign at $\gamma = 0$, for which we have a quantitative understanding of the Red Queen phase for $\gamma = 0$ (Section IV C). For $\gamma > \gamma_c \approx 0.65$, there is no steady state and Υ runs away to arbitrarily large values, but L remains roughly constant, and it is this L that is plotted as $\overline{L}$ for $\gamma > \gamma_c$ in Figure 15A. As in the linearized model, we expect weak dependence of $\overline{L}$ on Σ, and $\overline{\Upsilon} \sim \Sigma^2$ for gaussian $p(s)$.

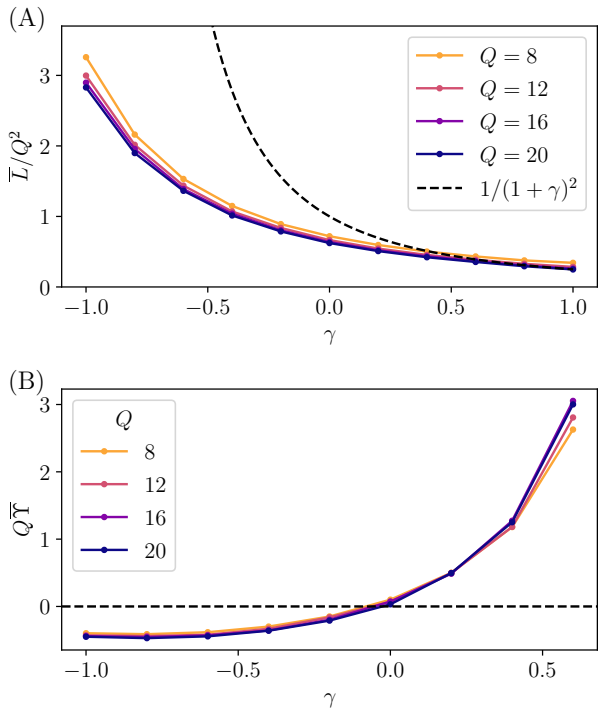

Figure 15. The Red Queen phase in the LV model depends on γ, with Q setting an overall scale for both $\overline{L}$ and $\overline{\Upsilon}$. (A) Steady state $\overline{L}$ in the LV model for $\Sigma = 0$ as a function of γ, scaled to coincide as expected for various Q. The dashed line shows the bound $\overline{L}/Q^2 = 1/(1+\gamma)^2$, which is known from $\hat{L}$ in the saturated assembled community. When $\gamma > \gamma_c \approx 0.65$ the oligarch phase obtains, though L remains roughly constant, as plotted here. (B) The dependence of $\overline{\Upsilon}$ on γ scales in the expected way ($\overline{\Upsilon} \sim 1/Q$) through the red queen phase, and begins to show deviations as the transition is approached. The dashed line shows the value of $\Upsilon = 0$ in the saturated assembled community. For $\gamma > \gamma_c$ there is no steady state, and $\overline{\Upsilon}$ is formally infinite. Here $\Sigma = 0$.

Appendix F: Transition with γ in LV model

As noted in the main text (Section III E), the LV model exhibits a transition in its evolutionary behavior before γ reaches unity. For $\gamma < \gamma_c \approx 0.65$ at $\Sigma = 0$, the lifetime distribution of strains looks exponential and the distribution of strain abundances remains fairly narrow, with the Red Queen phase presiding. For $\gamma > \gamma_c$, the oligarch phase takes over, there are strains which grow to comprise an $\mathcal{O}(1)$ fraction of the population, and the steady state in which p_{inv} is roughly constant breaks down, with Υ continuing to increase and the ecosystem becoming harder and harder to invade. The width of the crossover between these two phases appears to sharpen for increasing Q, indicating a sharp transition in the limit $Q \to \infty$.

The dynamics of Υ are discontinuous through the transition, with Υ plateauing for $\gamma < \gamma_c$ and increasing for $\gamma > \gamma_c$. This discontinuity suggests a first order transition, motivating our investigation of hysteresis around the critical γ. One can start the evolution with $\gamma > \gamma_c$, and, after some period of time, reduce γ to $\gamma < \gamma_c$. Figure 16A shows strain abundance trajectories during such a "quench." Here $\gamma = 1$ for the first 3×10^4 epochs of evolution, after which γ is reduced and the invader strains start to come in with $\gamma = 0.5$. The strains into which an $\mathcal{O}(1)$ fraction of the community have condensed start to decrease in abundance, but instead of going extinct and turning over, they reach an apparent steady state in which they fluctuate around their still-$\mathcal{O}(1)$ mean values. This behavior becomes rarer as the post-quench γ is decreased, indicating a region of phase coexistence around γ_c. Figures 16B–D show the dynamics of L, Υ and p_{inv} through this process, compared with the behaviors for $\gamma = 0.5$ and $\gamma = 1$ throughout the evolution. If one looks at the L, the hysteresis is not apparent, with L after the quench looking similar to L for a community that has always had $\gamma = 0.5$. However Υ and p_{inv} show clearly that the post-quench steady state is significantly different from a Red Queen state that has been evolving with $\gamma = 0.5$ from its beginning. The steady state that obtains after the quench displays properties of both the oligarch phase and the Red Queen phase, and may therefore be a useful toy model to better understand the oligarch phase.

Appendix G: Cavity calculation for assembled community

Here we carry out the cavity calculation for the assembled community in the linearized model: our results and approach are similar to that of ref. [20]. An analogous calculation for the LV model proceeds in a similar manner [18, 19, 22], and we summarize it at the end of this section. We consider a large community of strains at its fixed point, and add in another strain and resource, treating these as a small perturbation and then enforcing self-consistency between the statistics of this newly added strain and resource and the rest of the community. We will use the convention that repeated indices are summed over.

The strains obey the dynamical equation

$$\frac{\dot{\nu}_i}{\nu_i} = s_i + V_{ij}\nu_j - \Upsilon \tag{G1}$$

for $j \in \{1, \ldots, S\}$, where $V_{ij} = -G_{i\alpha}F_{j\alpha}$ for $\alpha \in \{1, \ldots, D\}$ and $\mathrm{E}[G_{i\alpha}F_{j\beta}] = \kappa\delta_{ij}\delta_{\alpha\beta}$. Υ is defined as $\Upsilon = \nu_i(s_i + V_{ij}\nu_j)$. Introducing quantities $R_\alpha = -F_{j\alpha}\nu_j$, the fixed point abundances satisfy

$$0 = s_i + G_{i\alpha}\tilde{R}_\alpha - \Upsilon, \quad \tilde{R}_\alpha = -F_{j\alpha}\tilde{\nu}_j, \tag{G2}$$

where tildes indicate the fixed point values prior to adding a new strain and resource. Now we add in a new strain and resource with fixed point abundances ν_0 and R_0 respectively. Defining quantities $\zeta_0 = G_{0\alpha}\tilde{R}_\alpha$ and $\phi_0 = -F_{j0}\tilde{\nu}_j$, we have

$$0 = s_0 + \zeta_0 + G_{0\alpha}\delta R_\alpha - \Upsilon, \quad R_0 = \phi_0 - F_{j0}\delta\nu_j, \tag{G3}$$

where we have defined local susceptibilities $\eta_\alpha = \frac{dR_\alpha}{d\phi_\alpha}$ and $\chi_i = \frac{d\nu_i}{d\zeta_i}$, and as a result the changes in R_α and ν_j are $\delta R_\alpha = -\eta_\alpha F_{0\alpha}\nu_0$ and $\delta\nu_j = \chi_j G_{j0}R_0$.

Assuming self-averaging, the new strain and resource abundances are

$$\nu_0 = \frac{\zeta_0 + s_0 - \Upsilon}{\kappa\eta}, \quad R_0 = \frac{\phi_0}{1+\kappa\chi}, \tag{G4}$$

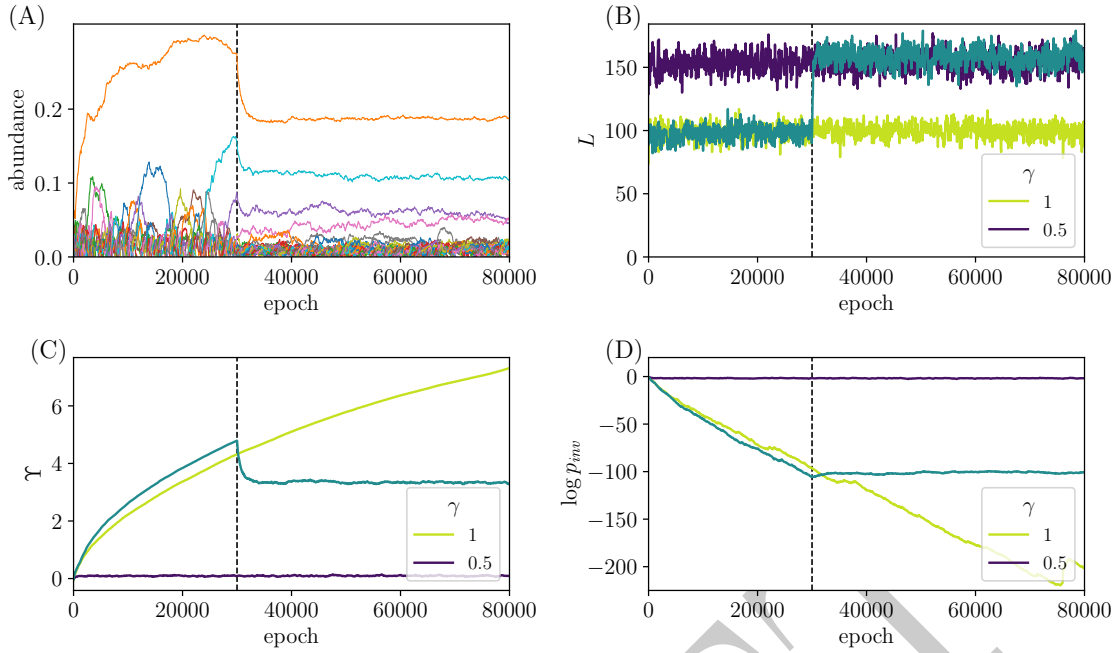

Figure 16. The transition between Red Queen and oligarch phases is first order, and exhibits hysteresis and phase coexistence when the system is tuned across the transition (A) Strain trajectories over the course of an evolution where initially $\gamma = 1$, and after 30000 epochs (at the vertical dashed line) evolution γ is "quenched" to $0.5 < \gamma_c \approx 0.65$. Nonetheless the system does not revert back to the steady state, with several long-lived strains persisting. (B) The trajectory of L over the same evolution (dark green), shown for comparison alongside L for constant $\gamma = 0.5$ and $\gamma = 1$. The value of L is indistinguishable in the post-quench phase and the Red Queen phase. (C)–(D) Dynamics of Υ and p_{inv} show a strong departure after the quench from their values when $\gamma = 0.5$ throughout. $Q = 20$ and $\Sigma = 0$.

where $\eta = \sum_\alpha \eta_\alpha$ and $\chi = \sum_i \chi_i$ are global susceptibilities.

Since ζ and ϕ are weighted sums of the G and F matrix elements respectively, they are gaussian distributed with mean 0. We will denote their variances as σ_ζ^2 and σ_ϕ^2 respectively. Let us take the s to be gaussian distributed with mean 0 and variance Σ^2, and define $\sigma_\xi^2 = \sigma_\zeta^2 + \Sigma^2$ and $Z = \Upsilon/\sigma_\xi$. We can now write self-consistency conditions for the variables σ_ϕ, σ_ξ, η, χ and Z, which require that the distributions of the added strain and resource abundances are the same as the distributions in the original community: in other words, Equation G4 is true for all strains, not just the cavity strain. Defining partial moments

$$W_m(Z) = \frac{1}{\sqrt{2\pi}} \int_0^\infty x^m e^{-(x+Z)^2/2} dx, \tag{G5}$$

our self-consistency conditions are

$$\chi = \frac{S}{\kappa\eta} W_0(Z) \tag{G6a}$$

$$1 = \frac{S\sigma_\xi}{\kappa\eta} W_1(Z) \tag{G6b}$$

$$\sigma_\phi^2 = \frac{S\sigma_\xi^2}{\kappa^2\eta^2} W_2(Z) \tag{G6c}$$

$$\eta = \frac{D}{1+\kappa\chi} \tag{G6d}$$

$$\sigma_\xi^2 = \frac{D\sigma_\phi^2}{(1+\kappa\chi)^2} + \Sigma^2. \tag{G6e}$$

These equations can be reduced to $SW_2(Z) = \kappa^2 D(1 - \frac{\Sigma^2}{\sigma_\xi^2})$, $\chi = \frac{SW_0(Z)}{\kappa(D - SW_0(Z))}$, $\eta = D - SW_0(Z)$ and $\sigma_\xi = \frac{\kappa(D - SW_0(Z))}{SW_1(Z)}$. Therefore we can obtain an equation for Z alone:

$$\frac{SW_2(Z)}{\kappa^2 D} = 1 - \left[\frac{\Sigma SW_1(Z)}{\kappa(D - W_0(Z))}\right]^2. \tag{G7}$$

A solution to these equations give us the distributions of the strain and resource abundances in the community, as well as the susceptibilities η and χ, and the scaled Lagrange multiplier Z. This mean field solution is expected to describe the unique stable uninvadable fixed point as long as it is stable to a small random perturbation on each of the strains' growth rates.

To look at the nonlinear instability that signals the breakdown of the mean field theory, we put a random field h_i on each of the biases and look at the change $\delta\xi_0$ in the bias of strain 0. We find that

$$\delta\xi_0 = \eta_\alpha G_{0\alpha} F_{j\alpha} \chi_j \delta\xi_j + h_0, \tag{G8}$$

where the sum is over both α and j. Then in evaluating the mean square of both sides of this equation we have

$$\mathrm{E}\left[(\eta_\alpha G_{0\alpha} F_{j\alpha} \chi_j \delta\xi_j)^2\right] = \sum_\alpha \eta_\alpha^2 \sum_j \chi_j^2 \,\mathrm{E}[\delta\xi_i^2]. \tag{G9}$$

Assuming that all the $\mathrm{E}[\delta\xi_i^2]$ are equal, since the strains are

statistically identical, we get

$$\mathrm{E}[\delta\xi^2] = \frac{\mathrm{E}[h^2]}{1-\sum_\alpha \eta_\alpha^2 \sum_j \chi_j^2} \tag{G10a}$$

$$\implies \sum_i \mathrm{E}[\delta\nu_i^2] = \frac{\sum_j \chi_j^2 \,\mathrm{E}[h^2]}{1-\sum_\alpha \eta_\alpha^2 \sum_j \chi_j^2} = \Xi \times \mathrm{E}[h^2] \tag{G10b}$$

where we have defined the *fragility* Ξ as the factor relating the variance of the random field to the sum of the squared changes in abundances that it produces. Since $\eta_\alpha = \eta/D$ and $\chi_j = \chi/SW_0(Z)$ in the mean field solution, we can write the fragility in terms of $L = SW_0(Z)$ as

$$\Xi = \frac{L/\kappa^2\eta^2}{1-L/\kappa^2 D} = \frac{LD}{(D-L)^2(\kappa^2 D - L)}. \tag{G11}$$

An instability signaling a phase transition occurs when the fragility diverges, at $L = \kappa^2 D$. This implies that the number of surviving strains is $\hat{L} = \kappa^2 D$ at the transition. Substituting this into Equation G7 tells us that $\hat{Z}$ is the solution to

$$\frac{W_2(\hat{Z})}{W_0(\hat{Z})} = 1 - \left[\frac{W_1(\hat{Z})\Sigma\kappa}{W_0(\hat{Z})(1-\kappa^2)}\right]^2. \tag{G12}$$

For $\Sigma = 0$, the solution to this equation is $\hat{Z} = 0$ and $\hat{S} = 2\kappa^2 D$. For $\Sigma \gtrsim 1$, we have $\hat{Z} \approx \frac{\Sigma\kappa}{1-\kappa^2}$ and $\hat{\sigma}_\xi \approx \Sigma$, meaning that $\hat{\Upsilon} \approx \frac{\kappa\Sigma^2}{1-\kappa^2}$ and $\hat{S} \approx \sqrt{2\pi}\kappa^2 D\hat{Z}e^{\hat{Z}^2/2} \sim \exp[\frac{\kappa^2\Sigma^2}{2(1-\kappa^2)^2}]$. The reciprocal of $\hat{S}$ gives us the invasion probability of the community at saturation. The scaling of these quantities at saturation of the assembled community is expected to be reflected in the Red Queen steady state.

Note that the linear susceptibility χ diverges when $L = D$. The nonlinear instability occurs for lower S than the linear instability for $\kappa < 1$, meaning that the cavity solution becomes invalid before it displays a linear instability. The nonlinear and linear instabilities occur in the same place for $\kappa = 1$, signaling the onset of the "shielded" phase when $\Sigma = 0$ [31]. When $\Sigma > 0$, $\hat{S}$ diverges for $\kappa \to 1$, indicating the marginality of the shielded phase.

We now summarize the cavity calculation for the LV model. In this case the cavity method yields, for the fixed point abundance of the cavity strain,

$$\nu_0 = \frac{\zeta_0 + s_0 - \Upsilon}{Q - \gamma\chi} \tag{G13}$$

where $\zeta_0 = \sum_j V_{0j}\tilde{\nu}_j$. The self consistency equations with gaussian distributed s_i of variance Σ^2 are then

$$\chi = \frac{S}{Q-\gamma\chi} W_0(Z) \tag{G14a}$$

$$1 = \frac{S\sigma_\xi}{Q-\gamma\chi} W_1(Z) \tag{G14b}$$

$$\sigma_\xi^2 = \frac{S\sigma_\xi^2}{(Q-\gamma\chi)^2} W_2(Z) + \Sigma^2 \tag{G14c}$$

where, as before, $Z = \Upsilon/\sigma_\xi$. The fragility is

$$\Xi = \frac{L}{(Q-\gamma\chi)^2 - L} \tag{G15}$$

and the susceptibility is

$$\chi = \frac{Q - \sqrt{Q^2 - 4\gamma L}}{2\gamma}, \tag{G16}$$

implying a divergence of Ξ at $\hat{L} = \frac{Q^2}{(1+\gamma)^2}$.

Appendix H: Exponential $p(s)$

In order to analyze the transient behavior of L as $\Delta(\Upsilon)$ (the local scale of the s_i distribution) decreases during the evolutionary transient, it is useful to investigate the behavior of the assembled community with an exponential distribution of the s_i given by $p(s) = \frac{1}{\Delta}e^{-s/\Delta}$. We define the variable $x_i \equiv s_i + \zeta_i$. The self consistency conditions then deal with the distribution of x_i, which is

$$p_x(x) = \frac{1}{\Delta}\exp\left[-\frac{x}{\Delta} + \frac{\sigma_\zeta^2}{2\Delta^2}\right]\Phi\left(\frac{x}{\sigma_\zeta} - \frac{\sigma_\zeta}{\Delta}\right), \tag{H1}$$

where Φ is the standard normal CDF. In particular, if we define partial moments

$$H_m(\Upsilon) = \int_0^\infty y^m p_x(y+\Upsilon)dy \tag{H2}$$

then our self consistency conditions can be written down in a similar fashion to those for the gaussian $p(s)$ in Equation G6. For the LV model, these conditions are

$$\chi = \frac{S}{Q-\gamma\chi} H_0(\Upsilon) \tag{H3}$$

$$1 = \frac{S}{Q-\gamma\chi} H_1(\Upsilon) \tag{H4}$$

$$\sigma_\zeta^2 = \frac{S}{(Q-\gamma\chi)^2} H_2(\Upsilon) \tag{H5}$$

For large Υ,

$$H_m(\Upsilon) \approx m! \times \Delta^m \exp\left[-\frac{\Upsilon}{\Delta} + \frac{\sigma_\zeta^2}{2\Delta^2}\right], \tag{H6}$$

and therefore for large Δ, we have $\chi \approx 1/\Delta$, implying that to leading order in Δ, the diversity is given by $L(\Delta) \approx Q/\Delta$. A similar analysis in the linearized model yields $L(\Delta) \approx \kappa D/\Delta$ for an exponential $p(s)$ with scale Δ. In particular, $\hat{\Upsilon}$ and $\hat{S}$ diverge for sufficiently large Δ, which scales as $(1+\gamma)^2/Q$ in the LV model and $1/\kappa$ in the linearized model—this is because Ξ cannot diverge when $L(\Delta) < \hat{L}$. Therefore sufficiently large Δ eliminates the unstable phase, for an exponential $p(s)$.

Appendix I: Diversity fluctuations in steady state

In the Red Queen steady state, L fluctuates around a mean value $\overline{L}$ which is proportional to D, with fluctuations that scale as $\sqrt{D}$, from rough independence of strains. In Figure 17A we see that the distribution of L/D concentrates as $D \to \infty$, and Figures 17B and C show that the both the mean and variance of L in the Red Queen steady state scale with D. This is consistent with expectations from the finite fragility of the Red Queen steady state.

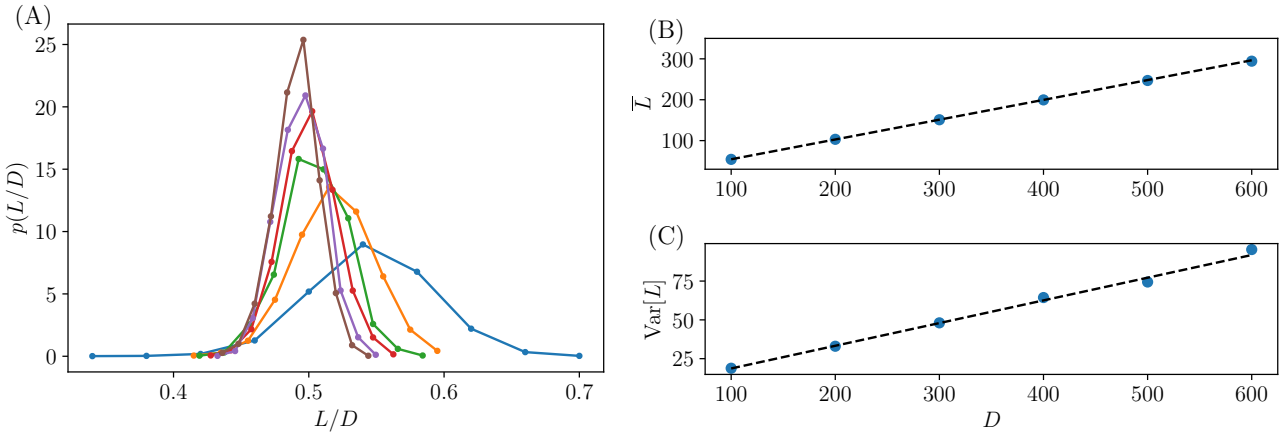

Figure 17. The scaling of the steady-state distribution of L with D in the linearized model. (A) From the distribution of L/D, we see that $\overline{L}/D$ approaches a D-independent value, as expected, while the distribution of L/D concentrates, indicating that fluctuations in L scale sublinearly with D in the Red Queen phase. (B)–(C) Both the mean and variance of L scale roughly linearly with D, which is consistent with the presence/absence of each strain being roughly independent random variables. For all panels, $\kappa = 0.8$, $\rho = 0$ and $\Sigma = 0$.

Appendix J: Evolutionary dynamical cavity analysis

Here we calculate the correlation function in Equation 10 and derive self-consistency conditions to find a statistical description of evolution in the LV model with $\gamma = 0$, $\Sigma = 0$.

Because of the absorbing boundary condition at $\zeta = 0$, we can use the solution of the Ornstein Uhlenbeck process together with the method of images to write down the distribution of $\nu(T)$ given that it started at some initial value $\nu(\mathbb{T})$ at invasion time $T = \mathbb{T}$. For simplicity we set $\mathbb{T} = 0$: integrating over $\mathbb{T}$—as we will later do—is the same as integrating over T. We use the fact that, for $\gamma = \Sigma = \overline{\Upsilon} = 0$, we have $\nu = \zeta/Q$. Therefore we can write the distribution of $\nu(T)$, conditioned on $\nu(0)$ and *nonextinction*, as

$$p(\nu(T)|\nu(0)) = \tag{J1a}$$

$$\frac{1}{\sqrt{2\pi}\sigma(T)}\left[\exp\left(-Q^2\frac{[\nu(T)-\nu(0)e^{-bT}]^2}{2\sigma(T)^2}\right) - \exp\left(-Q^2\frac{[\nu(T)+\nu(0)e^{-bT}]^2}{2\sigma(T)^2}\right)\right], \text{ where } \sigma^2(T) = \frac{J}{b}(1-e^{-2bT}). \tag{J1b}$$

We calculate the expectation $\langle\nu(T)\nu(T+\tau)\rangle$ over the joint distribution $p(\nu(T),\nu(T+\tau)|\nu(0))$, and integrate over all times $T \in [0,\infty)$ and over all $\nu(0) \in [0,\infty)$ distributed according to

$$p(\nu(0)) = \frac{c}{\sqrt{2\pi}\sigma_\infty}\exp\left[-\frac{Q^2\nu(0)^2}{2\sigma_\infty^2}\right]\Theta[\nu(0)], \tag{J2}$$

where we have introduced $\sigma_\infty = \sqrt{J/b}$ as the width of the incoming drive distribution, and c as setting the timescale for how often invasions enter the community. The integrals over T and $\nu(0)$ correspond to summing over all the strains in the community and can be done exactly, yielding

$$C(\tau) = \mathrm{E}[\langle\nu(T)\nu(T+\tau)\rangle]_{T,\zeta(0)} \tag{J3a}$$

$$= \frac{c\sigma_\infty^2}{4Q^2b}(1+2\log 2)e^{-b\tau}. \tag{J3b}$$

We now assert that the dynamics of the cavity drive are the same as those of the drives in the community. Since the cavity drive can fluctuate in sign, its correlation function is $C(\tau) = \sigma_\infty^2 e^{-b\tau}$, from an unconditioned Ornstein Uhlenbeck process at stationarity. Equating our two expressions for $C(\tau)$ gives

$$1 = \frac{c}{4Q^2b}(1+2\log 2). \tag{J4}$$

We can get another self-consistency condition by enforcing $\sum_j \nu_j = 1$. Note that $\langle\nu(T)|\nu(0)\rangle = \nu(0)e^{-bT}$. Then integrating this over the past and over the half-gaussian distribution of starting positions (as before) gives $c\sigma_\infty = Qb\sqrt{2\pi}$.

$\overline{L}$, the number of strains in steady state, is determined by the fact that the survival probability up to time T is $\langle\Theta[\nu(T)]|\nu(0)\rangle = \mathrm{erf}[Q\nu(0)e^{-bT}/\sqrt{2}\sigma(T)]$. Integrating over all past times and over the distribution of $\nu(0)$ gives $\overline{L} = \frac{c}{2b}\log 2$. Now we have two self-consistency conditions for b and σ_∞, along with an equation for $\overline{L}$:

$$c\sigma_\infty = Qb\sqrt{2\pi} \tag{J5}$$

$$4Q^2\frac{b}{c} = 1+2\log 2 \tag{J6}$$

$$\overline{L} = \frac{c}{2b}\log 2. \tag{J7}$$

We can solve these equations in terms of Q. The most easily testable prediction from numerics is

$$\overline{L} = \frac{2\log 2}{1+2\log 2} Q^2 \approx 0.58 \times Q^2, \tag{J8}$$

which agrees well with numerics for $\overline{L}$ with $\gamma = 0$ across a range of Q (Figure 9A). We also find that $\sigma_\infty = \sqrt{2\pi}\Omega/Q$, and $b = \Omega c/Q^2$ for $\Omega = \frac{1+2\log 2}{4}$, implying that $\sqrt{J} = \sqrt{2\pi c} \times \Omega^{3/2}/Q^2$. Therefore the theory prediction for the correlation function of the cavity drive is

$$C(\tau) = \frac{2\pi\Omega^2}{Q^2} \exp\left[-\frac{\Omega}{Q^2} c\tau\right]. \tag{J9}$$

Note that $c = 2$ if measuring time in successful invasions, since this makes the integral of the half-gaussian incoming drive distribution (and therefore the rate of incoming strains) equal to 1.

The distribution of strain lifetimes can be computed using known results from the theory of Ornstein Uhlenbeck (OU) processes—which can also be derived from the method of images. A useful result [52] is that the distribution of survival times $\mathcal{T}$ for an OU process $\dot{x} = -bx + \sqrt{2J}\eta(T)$ starting at position $x_0 > 0$ and ending when it hits the origin is

$$p_{\mathcal{T}}(\mathcal{T}|x_0) = \frac{2b^{3/2}x_0}{\sqrt{2\pi J}} \frac{e^{2b\mathcal{T}}}{(e^{2b\mathcal{T}}-1)^{3/2}} \exp\left[-\frac{bx_0^2}{2J(e^{2b\mathcal{T}}-1)}\right]. \tag{J10}$$

We can integrate over the distribution $p(x_0) = \frac{2}{\sqrt{2\pi}\sigma_\infty} e^{-x_0^2/2\sigma_\infty^2}\Theta(x_0)$, where $\sigma_\infty = \sqrt{J/b}$. We then obtain $p_{\mathcal{T}}(\mathcal{T}) = 2b/\pi\sqrt{e^{2b\mathcal{T}}-1}$, as quoted in Equation 14.

The steady state distribution of drives—and therefore of abundances—can also be computed from our self consistent solution. We expect that the drive distribution obeys a Fokker Planck equation (with the appropriate boundary conditions) that captures the dynamics of the drives from Equation 11 and includes a *source* term for incoming invaders. Therefore in the steady state, the condition for stationarity of the distribution $p(\zeta)$ is

$$b\sigma^2 p''(\zeta) + b[p(\zeta) + \zeta p'(\zeta)] + \frac{c}{\sqrt{2\pi}\sigma_\infty} \exp\left(-\frac{\zeta^2}{2\sigma_\infty^2}\right) = 0 \tag{J11}$$

with boundary conditions $p(0) = p(\zeta \to \infty) = 0$. Equation J11 contains the systematic and random parts in $\delta\zeta$ as well as the input from invading strains.

If we change variables to $z = Q\zeta = Q^2\nu$ and $N(z) = \frac{1}{Q^3}p(\zeta)$ so that $L = Q^2\int dz N(z)$, we find that the number density $N(z)$ of the rescaled abundances z obeys the Q-independent differential equation

$$2\pi\lambda^3 N''(z) + \lambda[N(z) + zN'(z)] + \frac{1}{2\pi\lambda} \exp\left(-\frac{z^2}{4\pi\lambda^2}\right) = 0 \tag{J12}$$

with $\lambda = \frac{1+2\log 2}{4}$. The solution to this equation with boundary conditions $N(0) = 0$, $N(\infty) = 0$ is plotted in Figure 10 as the theoretical prediction for the distribution of scaled abundances in the evolved community.

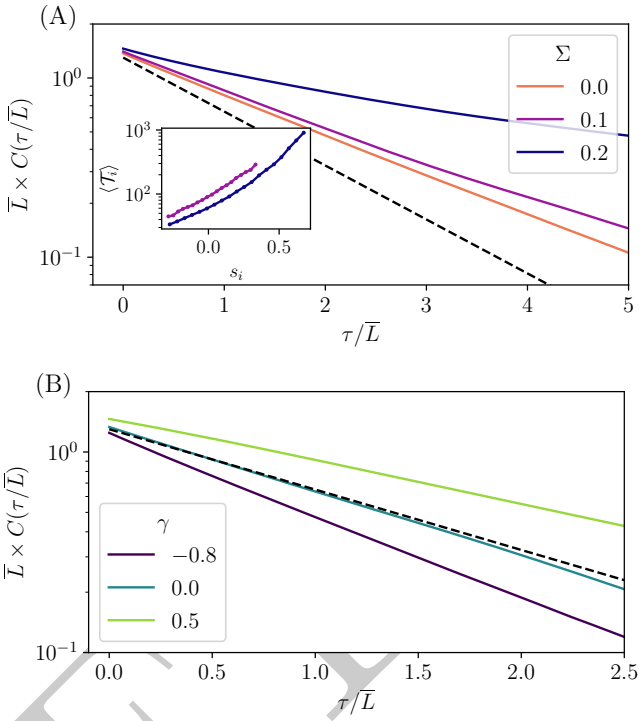

Figure 18. The correlation function $C(\tau)$ for various parameter choices. (A) The decay of $C(\tau)$ in the linearized model with $\kappa = 0.8$, for 3 different values of Σ is consistent with a power law when $\Sigma > 0$. The inset shows that the mean lifetime for a strain with general fitness s_i grows faster than exponentially in s_i. The dashed black line shows the theoretical result for the correlation function of the $\gamma = 0$ LV model. (B) In the LV model, with $\Sigma = 0$, increasing γ decreases the rate of decay of the correlation function, which corresponds to the fact that the community turns over faster for $\gamma < 0$ since invading strains will push existing strains extinct. The dotted black line is the same as in panel (A), with deviations from this result due to finite sampling in the numerics. In both panels we have normalized τ by a basic timescale of the community turnover given by $\overline{L}$, to isolate the effects of Σ and γ rather than an overall scaling by $\overline{L}$. For the linearized model the dependence of $\overline{L}$ on Σ is weak, as shown in Figure 4C, while for the LV model the dependence of $\overline{L}$ on γ is stronger, as shown in Figure 15.

Appendix K: $C(\tau)$ for nonzero γ and Σ

We expect that our solution for the evolutionary dynamics of the LV model at $\gamma = 0$ remains qualitatively valid across a range of parameters. Here we check that assumption by examining the correlation function $C(\tau) = \sum_{j=1}^{\overline{L}} \nu_j(T)\nu_j(T+\tau)$ for various Σ in the linearized model with $\kappa = 0.8$, and various γ in the LV model.

In Figure 18A we see that increasing Σ in the linearized model has the effect of decreasing the rate of decay of $C(\tau)$. In this case we expect the that $C(\tau)$ decays as a Σ-dependent power law due to the presence of rare high-fitness strains and their long residence times in the community. In the inset of Figure 18A we see that the mean lifetime of a strain grows faster than exponentially with its general fitness, indicating the large effect of strains with large s_i.

In Figure 18B we show that increasing γ increases the timescale of turnover as evidenced by slower decay of $C(\tau)$—with time rescaled appropriately by $\overline{L}$. However the correlation functions still look roughly exponential at large τ. For $\gamma < 0$ it appears that $C(\tau)$ decays slightly faster for small τ than for large τ, with the opposite trend for $\gamma > 0$.

We can understand the effect of the behavior for $\Sigma > 0$ through a toy model for evolution by independent invaders with $\Sigma > 0$. In the following toy model, the width of the extant s_i distribution is $\mathcal{O}(1)$ at steady state, as in the linearized model, in contrast to the $\mathcal{O}(1/Q)$ steady state width in the LV model.

We can try the same *Ansatz* that worked in the $\Sigma = 0$ and $\gamma = 0$ case, namely that the drives obey an Ornstein Uhlenbeck process, but now the absorbing boundary condition for strain i is at $\zeta = \overline{\Upsilon} - s_i$. Therefore strains with a sufficiently above-average s_i only go extinct when their drive becomes negative, which takes a time gaussian-long in $\overline{\Upsilon} - s_i$. In particular, defining $y_i = \overline{\Upsilon} - s_i$, we expect that the characteristic residence time in the community for strain i is $\langle \mathcal{T}_i \rangle \sim \frac{y_i^2}{J} e^{b y_i^2/4J}$. At large τ, the correlation function $C(\tau)$ will decay as the probability that a strain survives for time τ—therefore we need to integrate over the distribution of the y_i in order to get

$$C(\tau) \sim \int dy p(y) \exp\left[- \frac{J\tau}{y^2 e^{by^2/4J}} \right]. \tag{K1}$$

For $p(y) \sim e^{-\frac{1}{\psi}(y/\Sigma)^\psi}$, we find that for large τ,

$$C(\tau) \sim \exp\left[- \frac{1}{\psi} \left(\frac{2\sqrt{J/b}}{\Sigma} \right)^\psi \log^{\psi/2}\left(\frac{\Sigma^\psi b \tau}{2} \right) \right]. \tag{K2}$$

Therefore we see that an exponential *Ansatz* for correlation function of the dynamics is not self-consistent. In particular, this *Ansatz* yields that $C(\tau)$ decays as a Σ-dependent power law for a gaussian distribution of s (corresponding to $\psi = 2$). This result will change prefactors in the scaling of $\log\langle \mathcal{T}_i \rangle$ with y_i, but this scaling will still be quadratic due to the gaussian steady state of the unconditioned drive dynamics—and corresponding truncated gaussian distribution for the invader drive.

We expect that this general mechanism for producing long tails in the lifetime distribution—and therefore $C(\tau)$ is at work whenever $\Sigma > 0$. Having an upper limit for the s distribution (and therefore the y distribution) will cut off the power law at τ larger than the maximum $\langle \mathcal{T}_i \rangle$, beyond which the correlation function will look exponential. We have not pursued quantitatively testing these forms for $C(\tau)$ against our numerics due to unknown numerical factors that would affect the power scaling, as well as the lack of a self-consistent solution—but the results in Figure 18B indicate a broadening of the correlation function consistent with power law decay.

Appendix L: Comparison with results of de Pirey and Bunin

Recent work of de Pirey and Bunin [43] (dPB for short) has explored a Red Queen-like phase in a different context. dPB study *ecological dynamics* in a $\gamma = 0$ Lotka Volterra model with infinitesimal migration, such that there is a clear separation between strains which are extant and strains which would be extinct if not for the small migration. They find that if the diversity is high enough, the ecological dynamics are chaotic such that there are species which go nearly extinct before rising again to high abundance (rejoining the extant subset). Due to a separation of timescales arising from very small migration rate, the ecological dynamics therefore consist of a series of fixed points punctuated by changes that occur when a near-extinct species rises up to non-negligible abundance. When a species transitions from near-extinct to extant, the process is similar to an independent invader joining the community, as the abundance of the invader can jump up to a nonzero abundance determined by its ecological interactions with the extant community. This entrance to the community causes a change in the biases of the other strains in the community and therefore produces a steady state in which the abundance distribution is depleted at low abundance as compared to the truncated gaussian of the assembled community—indeed dPB find that their distribution at steady state is not well approximated by a truncated gaussian, and the number of extant species at any given time is less than the total capacity of an assembled community.

However, in the model studied by dPB, the steady state abundance distribution does not vanish at zero abundance. This is because when a species goes from extant to nearly-extinct, its probability of rejoining the extant community due to an ecological fluctuation is initially higher and then decays as its abundance gets closer to the lowest abundance permissible with the small migration. Therefore the boundary condition at zero abundance is not an absorbing one but rather a permeable boundary where species that hit zero abundance can be supported by infinitesimal migration and come back into the community soon after their extinction. dPB are able to write dynamical mean field equations for the abundance dynamics and solve these equations numerically to get the steady state abundance distribution. Our case is simpler in this respect since with *evolutionary dynamics* the extinction boundary is strictly absorbing. After guessing a form for the abundance trajectories and enforcing self-consistency, we find that a Markovian *Ansatz* for a purely exponential correlation function of the dynamics yields a self-consistent solution—which is not the case for dPB where the correlation function must be determined numerically according to self-consistency conditions. In our case, the equation satisfied by the abundance distribution is a boundary value problem (Equation J12) which can be solved numerically (Figure 10).

[1] Shinichi Sunagawa, Luis Pedro Coelho, Samuel Chaffron, Jens Roat Kultima, Karine Labadie, Guillem Salazar, Bardya Djahanschiri, Georg Zeller, Daniel R Mende, Adriana Alberti, et al. Structure and function of the global

ocean microbiome. *Science*, 348(6237):1261359, 2015.
[2] A framework for human microbiome research. *nature*, 486 (7402):215–221, 2012.
[3] Noah Fierer. Embracing the unknown: disentangling the complexities of the soil microbiome. *Nature Reviews Microbiology*, 15(10):579–590, 2017.
[4] Nadav Kashtan, Sara E Roggensack, Sébastien Rodrigue, Jessie W Thompson, Steven J Biller, Allison Coe, Huiming Ding, Pekka Marttinen, Rex R Malmstrom, Roman Stocker, et al. Single-cell genomics reveals hundreds of coexisting subpopulations in wild prochlorococcus. *Science*, 344(6182):416–420, 2014.
[5] Michael J Rosen, Michelle Davison, Devaki Bhaya, and Daniel S Fisher. Fine-scale diversity and extensive recombination in a quasisexual bacterial population occupying a broad niche. *Science*, 348(6238):1019–1023, 2015.
[6] R Frank Rosenzweig, RR Sharp, David S Treves, and Julian Adams. Microbial evolution in a simple unstructured environment: genetic differentiation in escherichia coli. *Genetics*, 137(4):903–917, 1994.
[7] Maren L Friesen, Gerda Saxer, Michael Travisano, and Michael Doebeli. Experimental evidence for sympatric ecological diversification due to frequency-dependent competition in escherichia coli. *Evolution*, 58(2):245–260, 2004.
[8] Benjamin H Good, Michael J McDonald, Jeffrey E Barrick, Richard E Lenski, and Michael M Desai. The dynamics of molecular evolution over 60,000 generations. *Nature*, 551 (7678):45–50, 2017.
[9] Richard E Lenski. Experimental evolution and the dynamics of adaptation and genome evolution in microbial populations. *The ISME journal*, 11(10):2181–2194, 2017.
[10] Steven E Finkel and Roberto Kolter. Evolution of microbial diversity during prolonged starvation. *Proceedings of the National Academy of Sciences*, 96(7):4023–4027, 1999.
[11] J Cesar Ignacio-Espinoza, Nathan A Ahlgren, and Jed A Fuhrman. Long-term stability and red queen-like strain dynamics in marine viruses. *Nature Microbiology*, 5(2):265–271, 2020.
[12] Marcia F Marston, Francis J Pierciey Jr, Alicia Shepard, Gary Gearin, Ji Qi, Chandri Yandava, Stephan C Schuster, Matthew R Henn, and Jennifer BH Martiny. Rapid diversification of coevolving marine synechococcus and a virus. *Proceedings of the National Academy of Sciences*, 109(12): 4544–4549, 2012.
[13] Angus Buckling and Paul B Rainey. Antagonistic coevolution between a bacterium and a bacteriophage. *Proceedings of the Royal Society of London. Series B: Biological Sciences*, 269(1494):931–936, 2002.
[14] Leigh Van Valen. A new evolutionary law. *Evolutionary theory*, 1:1, 1973.
[15] J Arjan GM De Visser and Joachim Krug. Empirical fitness landscapes and the predictability of evolution. *Nature Reviews Genetics*, 15(7):480–490, 2014.
[16] Daniel S Fisher. Inevitability of red queen evolution driven by organismic complexity and simple feedback via environmental modification. *bioRxiv*, pages 2021–09, 2021.
[17] Atish Agarwala and Daniel S Fisher. Adaptive walks on high-dimensional fitness landscapes and seascapes with distance-dependent statistics. *Theoretical population biology*, 130:13–49, 2019.
[18] Guy Bunin. Ecological communities with lotka-volterra dynamics. *Physical Review E*, 95(4):042414, 2017.
[19] Manfred Opper and Sigurd Diederich. Phase transition and 1/f noise in a game dynamical model. *Physical review letters*, 69(10):1616, 1992.
[20] Emmy Blumenthal, Jason W Rocks, and Pankaj Mehta. Phase transition to chaos in complex ecosystems with nonreciprocal species-resource interactions. *Physical Review Letters*, 132(12):127401, 2024.
[21] Valentina Ros, Felix Roy, Giulio Biroli, Guy Bunin, and Ari M Turner. Generalized lotka-volterra equations with random, nonreciprocal interactions: The typical number of equilibria. *Physical Review Letters*, 130(25):257401, 2023.
[22] Michael T Pearce, Atish Agarwala, and Daniel S Fisher. Stabilization of extensive fine-scale diversity by ecologically driven spatiotemporal chaos. *Proceedings of the National Academy of Sciences*, 117(25):14572–14583, 2020.
[23] Chi Xue and Nigel Goldenfeld. Coevolution maintains diversity in the stochastic kill the winner model. *Physical review letters*, 119(26):268101, 2017.
[24] Jef Huisman, Anna M Johansson, Eelke O Folmer, and Franz J Weissing. Towards a solution of the plankton paradox: the importance of physiology and life history. *Ecology Letters*, 4(5):408–411, 2001.
[25] Le Yan, Richard A Neher, and Boris I Shraiman. Phylodynamic theory of persistence, extinction and speciation of rapidly adapting pathogens. *Elife*, 8:e44205, 2019.
[26] Robert A Armstrong and Richard McGehee. Competitive exclusion. *The American Naturalist*, 115(2):151–170, 1980.
[27] Noam Shoresh, Matthew Hegreness, and Roy Kishony. Evolution exacerbates the paradox of the plankton. *Proceedings of the National Academy of Sciences*, 105(34):12365–12369, 2008.
[28] Peter Schippers, Antonie M Verschoor, Matthijs Vos, and Wolf M Mooij. Does supersaturated coexistence resolve the paradox of the plankton? *Ecology letters*, 4(5):404–407, 2001.
[29] Mikhail Tikhonov and Remi Monasson. Innovation rather than improvement: A solvable high-dimensional model highlights the limitations of scalar fitness. *Journal of Statistical Physics*, 172:74–104, 2018.
[30] Ada Altieri, Felix Roy, Chiara Cammarota, and Giulio Biroli. Properties of equilibria and glassy phases of the random lotka-volterra model with demographic noise. *Physical Review Letters*, 126(25):258301, 2021.
[31] Mikhail Tikhonov and Remi Monasson. Collective phase in resource competition in a highly diverse ecosystem. *Physical review letters*, 118(4):048103, 2017.
[32] Wenping Cui, Robert Marsland III, and Pankaj Mehta. Effect of resource dynamics on species packing in diverse ecosystems. *Physical review letters*, 125(4):048101, 2020.
[33] Robert Marsland III, Wenping Cui, and Pankaj Mehta. The minimum environmental perturbation principle: A new perspective on niche theory. *The American Naturalist*, 196 (3):291–305, 2020.
[34] Juan A Bonachela, Meike T Wortel, and Nils Chr Stenseth. Eco-evolutionary red queen dynamics regulate biodiversity in a metabolite-driven microbial system. *Scientific reports*, 7(1):17655, 2017.
[35] Jan Martin Nordbotten and Nils C Stenseth. Asymmetric ecological conditions favor red-queen type of continued evolution over stasis. *Proceedings of the National Academy of Sciences*, 113(7):1847–1852, 2016.
[36] Robert M May. Will a large complex system be stable? *Nature*, 238(5364):413–414, 1972.
[37] Aditya Mahadevan, Michael T Pearce, and Daniel S Fisher. Spatiotemporal ecological chaos enables gradual evolutionary diversification without niches or tradeoffs. *Elife*, 12: e82734, 2023.
[38] Anna Posfai, Thibaud Taillefumier, and Ned S Wingreen. Metabolic trade-offs promote diversity in a model ecosystem. *Physical review letters*, 118(2):028103, 2017.
[39] Rodrigo Caetano, Yaroslav Ispolatov, and Michael Doebeli. Evolution of diversity in metabolic strategies. *Elife*, 10:

e67764, 2021.

[40] Frédéric Vrins. Sampling the multivariate standard normal distribution under a weighted sum constraint. *Risks*, 6(3): 64, 2018.

[41] Sigurd Diederich and Manfred Opper. Replicators with random interactions: A solvable model. *Physical Review A*, 39 (8):4333, 1989.

[42] Giulio Biroli, Guy Bunin, and Chiara Cammarota. Marginally stable equilibria in critical ecosystems. *New Journal of Physics*, 20(8):083051, 2018.

[43] Thibaut Arnoulx de Pirey and Guy Bunin. Many-species ecological fluctuations as a jump process from the brink of extinction. *Physical Review X*, 14(1):011037, 2024.

[44] Felix Roy, Giulio Biroli, Guy Bunin, and Chiara Cammarota. Numerical implementation of dynamical mean field theory for disordered systems: Application to the lotka–volterra model of ecosystems. *Journal of Physics A: Mathematical and Theoretical*, 52(48):484001, 2019.

[45] Madeleine Bonsma-Fisher and Sidhartha Goyal. Dynamics of immune memory and learning in bacterial communities. *Elife*, 12:e81692, 2023.

[46] Jacopo Marchi, Michael Lässig, Aleksandra M Walczak, and Thierry Mora. Antigenic waves of virus–immune coevolution. *Proceedings of the National Academy of Sciences*, 118(27):e2103398118, 2021.

[47] Akshit Goyal, Leonora S Bittleston, Gabriel E Leventhal, Lu Lu, and Otto X Cordero. Interactions between strains govern the eco-evolutionary dynamics of microbial communities. *Elife*, 11:e74987, 2022.

[48] Takehito Yoshida, Stephen P Ellner, Laura E Jones, Brendan J M Bohannan, Richard E Lenski, and Nelson G Hairston Jr. Cryptic population dynamics: rapid evolution masks trophic interactions. *PLoS biology*, 5(9):e235, 2007.

[49] Mireia Valles-Colomer, Aitor Blanco-Míguez, Paolo Manghi, Francesco Asnicar, Leonard Dubois, Davide Golzato, Federica Armanini, Fabio Cumbo, Kun D Huang, Serena Manara, et al. The person-to-person transmission landscape of the gut and oral microbiomes. *Nature*, 614 (7946):125–135, 2023.

[50] Wei Zhou, Michelle Spoto, Rachel Hardy, Changhui Guan, Elizabeth Fleming, Peter J Larson, Joseph S Brown, and Julia Oh. Host-specific evolutionary and transmission dynamics shape the functional diversification of staphylococcus epidermidis in human skin. *Cell*, 180(3):454–470, 2020.

[51] Antonio M Martin-Platero, Brian Cleary, Kathryn Kauffman, Sarah P Preheim, Dennis J McGillicuddy, Eric J Alm, and Martin F Polz. High resolution time series reveals cohesive but short-lived communities in coastal plankton. *Nature communications*, 9(1):266, 2018.

[52] Luigi M Ricciardi and Shunsuke Sato. First-passage-time density and moments of the ornstein-uhlenbeck process. *Journal of Applied Probability*, 25(1):43–57, 1988.